Influence of hydrogen on the electrical resistivity of 4340 and 300M high-strength steels

Hosna Eftekhari

A Thesis

In The Department

Of

Mechanical, Industrial and Aerospace Engineering

Presented in Partial Fulfillment of Requirements

for the Degree of the Master of Applied Science (Mechanical Engineering)

at Concordia University

Montreal, Quebec, Canada

February 2025

CONCORDIA UNIVERSITY
SCHOOL OF GRADUATE STUDIES

This is to certify that the thesis prepared

By: Hosna Eftekhari

Entitled: Influence of hydrogen on the electrical resistivity of 4340 and 300M high-strength steels

and submitted in partial fulfillment of the requirements for the degree of

MASTER OF APPLIED SCIENCE in Mechanical Engineering

complies with the regulations of the University and meets the accepted standards with respect to originality and quality.

Signed by the final examining committee:

Chair:____
Dr. Hang Xu

Examiner:______________________________________
Dr. Hang Xu

Examiner:______________________________________
Dr. Sixu Deng

Supervisor:_____________________________________
Prof. Mamoun Medraj

Approved by: ____ Chair of Department
Prof. Martin Pugh

________2025 Dean of Faculty:___________________________________
Dr. Mourad Dabbabi

ABSTRACT

Influence of hydrogen on the electrical resistivity of 4340 and 300M high-strength steels

Hosna Eftekhari

Hydrogen embrittlement of steel components is a significant technological challenge, especially in the aerospace industry. Hydrogen is introduced into the steel during production and post-treatment. Trace quantities of hydrogen, as small as one-hundredth of parts per million, have the potential to induce embrittlement. Detection of hydrogen is not feasible by many conventional methods used to detect other elements as a result of its low atomic weight. Implementing a non-destructive method to measure hydrogen levels would greatly enhance the precision of quality control procedures. This study attempts to develop an approach for assessing hydrogen content in 4340 and 300M steel using electrical resistivity measurements. Specimens were charged with hydrogen using the electrochemical method and their hydrogen content was measured using thermal desorption spectroscopy. The change in resistivity was measured before and after hydrogen charging using the four-probe method. The findings reveal that the presence of hydrogen can be detected by the rise in electrical resistivity. To distinguish the impact of hydrogen on electrical resistivity from its effect on steel structure, the recovery of resistivity was measured after hydrogen desorption. The recovery of resistivity showed that hydrogen has an effect on electrical resistivity that is independent of microstructural damage seen in the absence of mechanical loading. This study illustrates that electrical resistivity measurement can potentially serve as the foundation for a novel, rapid, and non-destructive analytical technique for determining hydrogen content in high-strength steel components.

Acknowledgments

This thesis is dedicated to my parents for their unwavering support throughout my life. Their silent strength has spoken volumes, guiding me through every step of this journey. I also want to express my deep love and gratitude to my brother and sister, Adib and Saba, for always being there for me, even from afar.

To my dearest husband, Alireza, I am forever grateful for your dedication, endless love, and the time and resources you’ve devoted to supporting me. Your unwavering belief in me has been my anchor.

I would like to extend my heartfelt thanks to my supervisor, Professor Mamoun Medraj, for inspiring me not only professionally but also personally.

A special thanks to Dr. Rajwinder Singh, whose mentorship and inspiration have been pivotal throughout my research.

I would like to acknowledge Safran Landing Systems for generously funding my MSc research project.

Finally, I want to express my gratitude to my friends, who were like family to me.

Table of Contents

List of Figures VII

List of Tables X

Chapter 1: INTRODUCTION 1

  1-1 Problem statement 3

  1-2 Thesis layout 4

Chapter 2: LITERATURE REVIEW 5

  2-1 Hydrogen absorption and diffusion in steel 5

  2-2 Hydrogen interactions with steel microstructure 10

  2-3 Hydrogen embrittlement and mechanical susceptibility 14

  2-4 Effect of hydrogen on the electronic structure of steel 16

  2-6 Resistivity of steel in the presence of hydrogen 19

    2-6-1 Classic and quantum mechanics approach 19

    2-6-2 Four-probe method for resistivity measurement 26

  2-7 Objectives 31

Chapter 3: EXPERIMENTAL PROCEDURES 32

3-1 Steel sample materials and preparation ... 32

3-2 Electrochemical hydrogen charging ... 33

3-3 Resistivity measurement using the Four-probe method (DC) ... 35

3-4 Hydrogen content measurement ... 36

3-5 Characterization ... 37

Chapter 4: RESULTS AND DISCUSSION ... 37

4-1 Effect of hydrogen on the electrical resistivity of 4340 and 300M ... 38

4-2 The multifaceted effects of hydrogen ... 43

4-2-1 The impact of microstructure and composition on hydrogen-induced change in electrical resistivity of 4340 and 300M ... 43

4-2-2 Recovery in resistivity after hydrogen desorption ... 53

4-3 Isolated effect of solute hydrogen on resistivity ... 55

Chapter 5: CONCLUSIONS ... 60

5-1 Original contributions ... 61

5-2 Future work ... 61

References ... 62

List of Figures

Figure 1. Schematic of hydrogen embrittlement mechanisms [79] 16

Figure 2. Change in impedance as a function of hydrogen content [17] 25

Figure 3. Changes in eddy current signal and embrittlement index [16].................................... 25

Figure 4. (a) Two-probe method and, (b) four-probe method and resistances, (c) four-point probe showing probe distances and current flow [101] 28

Figure 5. The correlation between resistivity and hydrogen content [18] 29

Figure 6. SEM images of final martensitic microstructures of (a) 4340 and (b) 300M, used in this research 20.0 µm 33

Figure 7. Schematic of electrochemical cathodic charging [107]... 33

Figure 8. Raw data showing voltage-time graph for a non-charged 4340 specimen measured at 200mA.. 36

Figure 9. (a) The resistivity measurement setup and (b) hydrogen content analyzer 37

Figure 10. Voltage - Current graph for a 4340 specimen before and after hydrogen charging in 0.5 M H_2SO_4 containing NH_4SCN, at the current density of 100 mA/cm^2 39

Figure 11. Change in resistivity as a function of charging time for (a) 4340 and (b) 300M, hydrogen charged in 0.5 M H_2SO_4 containing 3 g/l NH_4SCN, at the current density of 100 mA/cm^2 40

Figure 12. Percentage change in resistivity with charging time for 4340 and 300M, hydrogen charged in 0.5 M H_2SO_4 containing 3 g/l NH_4SCN, at the current density of 100 mA/cm^2 41

Figure 13. Percentage change in resistivity as a function of hydrogen content for (a) 4340 and (b) 300M hydrogen charged in 0.5 M H_2SO_4 containing 3 g/l NH_4SCN, at the current density of 100 mA/cm^2 42

Figure 14. (a) The EBSD and the inverse pole figure map (IPF-Z) of martensitic 4340 operated at 25 kV parallel to the Z direction shows grain boundaries and martensite lath blocks. The stereographic triangles for BCT and Fe_3C are shown (b) Hierarchy in a martensitic microstructure [112]. (c) The EBSD map showing the Austenite and cementite at the lath boundaries of non-charged 4340 45

Figure 15. The EBSD and the inverse pole figure map (IPF-Z) of martensitic 300M operated at 25 kV parallel to Z direction. The stereographic triangles for BCT and Fe_3C. (b) Austenite and cementite at the lath boundaries of non-charged 300M 46

Figure 16. A blister wall crack in 4340, hydrogen charged for 4 hours in 0.5 M H_2SO_4 containing 3 g/l NH_4SCN, at the current density of 100 mA/cm^2. (a) OM image, (b) SEM image 46

Figure 17. Optical microscopic images of 300M charged for (a) 2, (b) 4 and (c) 7 hours, in a 0.5 M H_2SO_4 solution containing 3 g/l NH_4SCN, at the current density of 100 mA/cm^2 47

Figure 18. Cu-containing precipitates at crack initiation points in hydrogen-charged 4340 steel(a) across the crack containing oxygen, (b) along the crack containing sulfur 49

Figure 19. EDS mapping of crack in hydrogen-charged 4340 steel showing copper and sulfur concentrations along the crack opening. 50

Figure 20. (a) Cracked inclusion primarily composed of Al and O in 300M steel, highlighting a potential crack initiation site due to its composition, (b) Aluminum-rich precipitate located close to a crack in 300M steel. 51

Figure 21. Percentage recovery of resistivity with time for (a) 4340 and (b) 300M hydrogen charged in 0.5 M H_2SO_4 containing 3 g/l NH_4SCN at 100 mA/cm^2 54

Figure 22. Electrical resistivity of 300M as a function of charging time. Specimens were charged in 0.1 M H_2SO_4 at 100 mA/cm^2 57

Figure 23. Percentage change in resistivity of 300M as a function of charging time. Specimens were charged in 0.1 M H_2SO_4 at 100 mA/cm^2 58

Figure 24. Hydrogen content as a function of percentage change in resistivity for 300M specimens charged in 0.1 M H_2SO_4 at 100 mA/cm^2 58

Figure 25. Percentage recovery of resistivity in each charging time for 300M hydrogen charged in 0.1 M H_2SO_4 at 100 mA/cm^2 59

List of Tables

Table 1. Reversible and irreversible traps in steel alloys [3] 10

Table 2. Chemical composition of 4340 and 300M steels (wt %) 32

Chapter 1: INTRODUCTION

Hydrogen embrittlement (HE) has drawn the attention of researchers in many industries due to its adverse effects on the durability of industrial parts. Steel components used in contemporary applications including transportation, construction, and aviation are subject to this phenomenon [1]. Hydrogen is introduced into steel not only through manufacturing processes but also during the post-treatments such as electroplating and during service [2].

In recent years hydrogen fuel has gained prominence within refining and energy sectors, owing to its inherent characteristics as a lightweight, storable, and energy-dense resource, while simultaneously offering the advantage of emitting no direct pollutants or greenhouse gases. As a result of this popularity, HE of the fuel tanks and other iron-based alloys and guaranteeing their durability have been in the spotlight [3].

High-strength steels are more prone to HE than others even for hydrogen contents as small as a tenth of parts per million [3,4]. Steel alloys such as 4340 and 300M find applications in the aerospace sector, especially, for manufacturing critical components such as landing gears and helicopter transmission shafts [5,6]. HE poses risks for such steels and the evaluation tests need to be designed based on the application of the component in service. Thermal desorption spectroscopy (TDS) is used to quantify the hydrogen content in the material. Measurement of mechanical characteristics such as tensile strength [7], ductility [8], fracture toughness [9] and fatigue crack growth [8] enables the detection and assessment of the impact of hydrogen on the mechanical properties of high-strength steels. In general, the investigation into the deterioration of the mechanical properties of steel is based on exploring the underlying mechanisms of HE. These investigations involve a meticulous analysis of the fractured surfaces of the failed specimens to identify the root causes behind the degradation. Various mechanisms have been suggested by researchers for HE such as Hydrogen-Enhanced Localized Plasticity (HELP) [10], Adsorption Induced Dislocation Emission (AIDE), Hydrogen-Enhanced Decohesion (HEDE), and Hydrogen-Enhanced Strain-Induced Vacancies (HESIV) [9,11–13].

Measurement of mechanical properties is a reliable approach to HE evaluation. However, these measurements are destructive. Investigation of physical properties can be an alternative to the existing testing techniques. The development of such a technique requires a deep understanding of the electron structure of materials. The effect of hydrogen on electron structure [14], vacancies and dislocations [15] within BCC iron and steel have been investigated using first-principles calculations. These investigations indicate a local increase in the density of states [15] and therefore in the number of free electrons. The effect of hydrogen on vacancies and dislocations can potentially influence the electrical resistivity of steel components. This paved the way for the viewpoint that hydrogen content can impact the physical properties of steel. Exploring the measurement of physical properties in hydrogen-affected steel can establish the foundation for evaluating hydrogen content using non-destructive testing methods which allows for possible quantification of hydrogen content in a component in between services.

Potentially, HE can be indirectly quantified through the measurement of material characteristics that exhibit sensitivity to hydrogen content and are measurable without causing damage to the specimen. Previous studies demonstrated a correlation between variations in hydrogen content and physical properties such as magnetic properties [5,16,17], and electrical resistivity [18], within both energy storage materials and steel [19,20].

Some researchers have investigated the correlation between the hydrogen effect and changes in the physical properties of steels by non-destructive methods. Koenig et al. [17], and Lasseigne et al. [21] measured resistivity indirectly and Zhou et al. [18] proposed setups based on electromagnetic measurements and showed the change in measured parameters as a function of hydrogen content [18,22].

1-1 Problem statement

As previously mentioned, the primary approach for detecting the presence of hydrogen involves mechanical testing and quantitative measurements obtained through TDS. Additionally, by investigating the fracture surface and tracing fracture features back to possible mechanisms, it is possible to indirectly identify defects induced by hydrogen. While these methods provide valuable insights into the presence of hydrogen, their downside lies in the destruction of specimens.

A potential solution to this challenge is being pursued by examining the change in the physical properties of hydrogen-charged steel. Studies have revealed that the electrical resistivity of X65 pipeline steel increases following electrochemical hydrogen charging [17,18,21]. Some researchers have attempted to develop a non-destructive method for hydrogen detection using electrical resistivity [17,21], though few provided sufficient detail in their studies [18]. It has been observed that the change in the electrical resistivity of 4340 steel following hydrogen charging is minimal, falling within acceptable error margins [22]. Consequently, detecting hydrogen in 4340 steel using this method was considered impractical [22]. Thus, the current study explores the magnitude of electrical resistivity changes in 4340 and 300M due to hydrogen charging. Through the analysis of resistivity measurement and the attributed hydrogen content, this research aims to deepen our understanding of the early detection of hydrogen and prevention of HE in steel components.

1-2 Thesis layout

The introduction outlines the issue of HE in steels and briefly explores the history of previous research on this matter. Subsequently, the following chapter provides a more detailed explanation of the source of hydrogen in the material, HE mechanisms and their relation to the electron structure of steels. Further on, microstructural features, the influence of hydrogen on them, and the overall impact of hydrogen on the physical properties of steel have been examined. Chapter 2 expands further upon previous research conducted on HE evaluation using methods based on physical properties. Chapter 3 will detail the methodology, such as sample preparation procedures, hydrogen charging technique, resistivity measurement, and hydrogen content evaluation. Chapter 4 discusses the results of resistivity measurements in relation to hydrogen content, supported by electron and optical microscopy, as well as electron dispersive spectroscopy (EDS) and electron backscatter diffraction (EBSD) technique. The final chapter summerizes the findings and contributions of this study while offering recommendations for future research.

Chapter 2: LITERATURE REVIEW

The first part of this chapter outlines how hydrogen enters and diffuses within steel. With this understanding, this study delves into the adverse effects of hydrogen on the steel structure. Next, it is examined whether the effects of hydrogen are limited to mechanical properties or extend significantly to physical properties. A detailed explanation is then offered for using the four-probe method to measure electrical resistivity, a property potentially influenced by hydrogen.

2-1 Hydrogen absorption and diffusion in steel

Understanding the absorption and trapping of hydrogen atoms within steel crystal structures is essential for analyzing how variations in hydrogen content affect the properties of the material. Hydrogen interactions with steel structure can cause HE which is defined as the reduction of mechanical strength and ductility as a result of hydrogen absorption and diffusion [10,21,23]. HE is particularly severe in high-strength steels, significantly affecting their mechanical properties. The mechanisms responsible for such effects are discussed in the next sections. The impact of hydrogen on physical properties, potentially influenced by changes in electron structure, is examined in the following section. Another crucial aspect is hydrogen concentration, which determines the extent of its influence on various properties. The amount of absorbed hydrogen is influenced by steel composition, microstructure, and applied stress under ambient pressure and temperature conditions. As steel strength increases, its susceptibility to low levels of hydrogen rises [24]; hydrogen quantities of as small as 0.02 wt ppm can affect the yield strength of AISI 4340 steel [25,26]. Kim et al. [27] reported a susceptibility threshold ranging from 0.07 to 0.2 wt ppm in a high-strength steel with a tempered martensitic microstructure.

In industrial settings, sources of hydrogen include manufacturing process [28] cathodic protection, electroplating [29], corrosion [30], etc. For experimental studies, hydrogen can be introduced into steel using various methods such as electrochemical cathodic charging [31] and high-pressure thermal charging [32]; in this thesis, electrochemical cathodic charging under ambient pressure and temperature was employed. Keeping the experimental conditions constant, the effect of hydrogen on the physical properties of steel without changing parameters such as grain size and microstructure was investigated. During cathodic charging in an acidic solution, some hydrogen ions are produced through water hydrolysis and some exist in the solution as H^+ ions. The ions are adsorbed to the cathodic metal surface and bond with other hydrogen atoms to form hydrogen gas molecules and leave the metal surface or dissolve into the steel, and are absorbed into the bulk [33]. Once absorbed, hydrogen atoms assemble at internal defects such as dislocations, voids, inclusions, grain boundaries, etc., where they may combine to create hydrogen molecules, as in Eq. 1 and Eq. 2.

$$\mathrm{H^{+}+e^{-}=H_{ads}} \qquad \text{Eq. 1}$$

$$\mathrm{2H_{ads}=H_2} \qquad \text{Eq. 2}$$

Hydrogen is adsorbed in atomic form on the steel surface via physisorption or chemisorption. Its interaction with steel microstructure depends on its electronic configuration. When the energy of dissociation is supplied, hydrogen is dissociated into a proton and an electron. The proton occupies an interstitial site directly beneath the surface, while the 1s electron goes into the d-band of the host metals such as iron [34–36]. In the metallic environment, conduction electrons in the Fermi level screen the proton at short distances by neutralizing the charge [35]. In ambient temperature and pressures, the solubility of hydrogen highly depends on the microstructure of steel which varies with heat treatment and mechanical work [37,38]. The packing factor is a parameter that can affect the diffusivity and solubility of hydrogen atoms. BCC has a lower packing factor of 0.68 compared to that of FCC (0.74), making FCC more compact. In FCC, the activation energy for trapping is lower than the energy required for diffusion, facilitating easier trapping and de-trapping. Conversely, the diffusivity of hydrogen in BCC lattice is higher and solubility is lower than in an FCC crystal structure [39,40].

The solubility of hydrogen in interstitial sites is controlled by electron interaction energy between the site and the hydrogen atom [41]. This energy is known as the binding energy and will be discussed in the following sections. In BCC iron, hydrogen prefers to occupy tetrahedral sites. The presence of hydrogen in the lattice interstitial site can increase its size [35]. These sites have a larger radius of 0.36 Å as compared to octahedrals with a radius of 0.19 Å. It is only at high temperatures and pressures that hydrogen diffuses into octahedral sites and the solubility can reach a saturation threshold of tens of wt ppm in steel [14]. Jiang et al. [14] used DFT to study the adsorption and diffusion of hydrogen atoms into the BCC iron lattice and reported the preferred sites for hydrogen to be below the planes of (110) and (100) which have the smallest surface energy in α-iron. In the absence of traps, hydrogen prefers to stay on the surface rather than in the bulk, since moving to subsurfaces requires energy, and it takes very little energy for hydrogen to move from the bulk to the surface.

At ambient pressure and temperature, hydrogen absorption in the mentioned spots and the defects has a solubility limit that depends on the charging method, steel composition, and microstructure. Using cathodic charging, Shim et al. [42] reported a saturation value of approximately 5 to 8 wt ppm for AISI 4340. However, saturation values can vary with charging conditions. Elevated temperature, pressure, as well as severe electro-charging can enhance hydrogen diffusion, leading to supersaturation in the metal and the formation of molecular hydrogen in discontinuities [42]. In electrochemical charging, excess hydrogen in iron may be accommodated through interstitial dissolution, segregation at lattice imperfections, precipitation in microcavities, or adsorption at cavity surfaces. The diffusion rate of hydrogen in iron is significant even at room temperature, allowing interaction between interstitially dissolved hydrogen and lattice imperfections, resulting in an equilibrium between dissolved and undissolved hydrogen states. Changes in temperature and lattice imperfections shift this equilibrium [43]. At higher temperatures and pressures, hydrogen solubility increases. At certain conditions, interstitial trap sites can also absorb hydrogen as H_2 gas [44,45]. Soluble hydrogen is trapped in microstructural features, classified into two primary types based on their binding energies: permanently retaining and reversibly trapped hydrogen, as in Table 1 [3]. Inclusions are potentially strong hydrogen traps in steels such as 4340 whereas carbide interfaces are comparatively lower energy traps [46]. The interactions between hydrogen and these features are a key point in the material performance in a hydrogen-rich environment. Several experimental techniques such as electrochemical permeation testing and TDS have been used to study hydrogen diffusion in metals and alloys with diverse microstructures [47–49]. These methods detect hydrogen adsorption rates, diffusivity, and trap binding energy by measuring hydrogen permeation and release during charging and heating. However, interpreting results is challenging due to complex microstructures and sensitivity to experimental parameters such as charging current and specimen geometry. To address these challenges, modeling frameworks have been developed to quantitatively investigate hydrogen-microstructure interactions in materials [50–53].

The apparent diffusivity of hydrogen may vary even in two specimens with identical microstructures and compositions in Fe-C-Mo martensitic steel, according to Frappart et al. [47]. This discrepancy arises from differences in the number of trap sites, as well as their binding energy and activation energies for permeation. This idea is related to the apparent diffusion coefficient and lattice or interstitial hydrogen diffusion, which can vary within different regions of the same material, consequently, leading to regional differences in hydrogen concentration [47]. Traps are classified according to their trapping energy and host steel alloys.

Due to slight differences in composition and heat treatment temperatures, 4340 and its modified version 300M, exhibit different trapping energies and diffusivity because of their microstructural features. The diffusion coefficients (D) in 4340 and 300M are remarkably different; D_{300M} = 8.8 $\times 10^{-12}\ m^2$/s and D_{4340} = 2 $\times 10^{-11}\ m^2$/s [29,54]. The diffusion coefficient of 300M is lower than that of 4340. This difference can be as a result of the different carbide characteristics in the microstructures (type and composition) which originate from the alloying elements. The alloying elements can affect the material in both electron and atomic aspects. The microstructure of heat-treated AISI 4340, according to ASTM F519 [55], contains martensite laths structured in austenite prior grain boundaries and iron carbides are in the form of cementite. Grain boundaries and cementite are the diffusivity paths and potential trap sites for hydrogen [41,47,56,57]. However, 300M undergoes a heat treatment at a higher temperature and contains some reverted austenite which can be due to its higher Ni content. It also contains ε-carbide at lath boundaries as a result of heat treatment due to the silicon content being twice as much as that in 4340 [58]. Due to these differences, the two steel alloys may show distinct behaviors in response to hydrogen absorption and diffusion. It is explained in the next section how hydrogen interacts with the microstructural features of steel. Subsequent sections aim to establish the relationship between microstructural features and hydrogen, and their impact on physical properties.

Table 1. Reversible and irreversible traps in steel alloys [3]

Type of trap	Activation Energy (kJ/mol)	Material
Reversible Hydrogen-trapping sites		
Grain boundary	17.2	Fe
Grain Boundary, Dislocation	21-29	4135, iron, Martensitic bolt steel
Deformation field around Dislocation	29 ± 5	Ferritic steel
Irreversible Hydrogen-trapping sites		-
Semi coherent TiC	49.9	0.05C-0.22Ti-2.0Ni steel
High-angle Grain Boundary	53-59	Range of steel alloys
NbC interface	63-68	Range of steel alloys
Incoherent TiC	85.7, 86.9	0.05C-0.22Ti-2.0Ni steel

2-2 Hydrogen interactions with steel microstructure

Hydrogen atoms introduced into steel coexist with alloying elements and the microstructural features of the iron-based alloy. To clarify how hydrogen remains and diffuses in steel, it is crucial to recognize the short-range and long-range interactions between these atoms and the microstructural features. Additionally, understanding these interactions at the electron level can provide deeper insights into the explanation of changes in physical properties such as electrical resistivity due to hydrogen. As explained in the previous section, the hydrogen effects on steel structure can vary with the charging method.

Hydrogen in the metallic bulk is considered to be in an electron cloud [59]. Hydrogen atoms diffuse into monovacancies or are distributed in vacancy clusters all over the BCC iron lattice [2,60]. First-principles calculations show that despite the repulsion of ions, the monovacancy could accommodate up to six hydrogen atoms due to their compact radius, thereby impacting the electron state configurations of the host iron atoms [61]. The investigation done by Ohsawa et al. [61] delved into the variability of stable hydrogen atom positions within the monovacancy, depending upon the number of hydrogen atoms present. A vacancy traps hydrogen atoms by creating a charge density, and promoting the binding of hydrogen clusters on its internal surface. Such a vacancy can expand to accommodate more hydrogen atoms and H_2 gas [62]. Ab initio calculations show that vacancies and hydrogen interactions significantly increase the equilibrium vacancy concentration in Fe-H alloys, particularly at lower temperatures [60]. However, the diffusion of vacancies in iron diminishes considerably below 500–600 K, potentially limiting changes in equilibrium vacancy concentration. In contrast, hydrogen atoms remain highly mobile at these lower temperatures, especially at grain boundaries. The concentration of hydrogen atoms bonded with vacancies remains relatively small, indicating limited efficiency in trapping hydrogen across different concentrations and temperatures [60]. The presence of multiple hydrogen atoms in a monovacancy can be justified through long-range ordering and in the presence of other atoms. McEniry et al. [63] explain the mechanism enabling hydrogen accumulation, where hydrogen diffuses into the subsurface and accumulates along discontinuities despite repulsion during electrochemical charging. They [63] have used atomistic modeling for the Fe-C-H system and reported that hydrogen atoms occupying adjacent void sites near the edge dislocation experience repulsive interactions for the nearest neighbor and negligible interactions for the second nearest neighbor. Hydrogen-hydrogen interactions between voids parallel to the grain boundary plane are minimal due to the greater distance between void sites in this direction. In the case of voids and hydrogen, long-range attraction and short-range repulsion are the main forces. When considering the hydrogen atoms and alloying elements, the type and amount of forces depend on the size and type of the element [63]. Carbon in the form of cementite is a strong trap for hydrogen [64]. It can affect hydrogen accumulation in atomic form as well. Carbon present at a void site may attract hydrogen to an adjacent one. This occurs because the local strain induced by the carbon atom slightly increases the displacement between the two grains, resulting in a small increase in available volume for hydrogen at the adjacent void, leading to enhanced hydrogen solubility. Consequently, carbon atoms may amplify hydrogen concentration at nearby vacant interstitial sites for this category of tilt grain boundaries [63].

Marrow et al. [65] and Terasaki et al. [66] showed void initiation at slip bands or cell walls because of vacancies. As more void formation is facilitated, clusters of voids can form. In the case of hydrogen electrochemical charging, the fugacity of hydrogen gas is high on the charging surface. In this case, the concentration of hydrogen may segregate towards grain boundaries and particle interfaces. In other words, the equilibrium can shift towards the right side in Eq. 2, which results in the production of H_2 gas. This might entail the build-up of pressure from molecular hydrogen gas within the less constrained grain boundary areas before subjecting the material to any mechanical loading. The accumulation of hydrogen can lead to the development of enduring defects such as voids, blisters, and visible cracks within the microstructure, with cracks and blisters predominantly emerging on or near the surface [42,67].

Although HE occurs even with minimal hydrogen, researchers have used high fugacity charging to study the effects on Fe-based crystal structures. Allen Booth and Hewitt [68] developed a model that explains the behavior of hydrogen in both molecular and atomic forms within iron and steel microstructures. Calculations were based on hydrogen diffusion in voids, considered as trap sites. It was assumed that atomic and gaseous hydrogen are interconvertible. Given that hydrogen is trapped in voids, it was proposed that the hydrogen diffusion coefficient depends on the number of trap sites. Equations demonstrated that apparent diffusivity decreases with an increased volume concentration of voids. Thus, hydrogen is trapped in its two forms within voids rather than diffusing through the metallic lattice [68]. According to Oriani [35], voids and microcracks are formed to release the stress caused by high hydrogen pressure. However, signs of transgranular fracture in the fracture interface have been detected as the fugacity of hydrogen increases, according to Shim et al. [42]. Hydrogen can cause permanent damage in specimens charged with high fugacity hydrogen. Although aging at room temperature reduces the risk of transgranular and brittle fracture, it does not prevent these fractures, with cracks forming during aging. Thus, hydrogen-induced damage can persist in steel after hydrogen desorption, even though desorption may alleviate the loss of ductility [69]. To release hydrogen, electro-plated steel components undergo a heat treatment known as baking, where the plated material is heated to 190-200°C for up to 24 hours [70].

The effect of hydrogen on steel is typically demonstrated through mechanical testing and fracture surface analysis. While research on mechanical properties is extensive, further exploration of HE mechanisms can enhance the insight into the interaction of hydrogen with the steel electron structure. The next two sections briefly explain HE mechanisms and the effect of hydrogen on the electronic structure of steel. This can serve as a foundation for connecting the behavior of hydrogen with the physical properties of steel.

2-3 Hydrogen embrittlement and mechanical susceptibility

The impact of HE on the mechanical properties has been a topic of extended studies, leading to several proposed mechanisms. However, a complete comprehension of these mechanisms remains unknown with the detection of HE standing out as one of the most challenging aspects. HE can occur through a few primary mechanisms, each representing distinct behaviors of the material, the HEDE, HELP, AIDE, and HESIV mechanisms [2]. A schematic of the mechanisms is shown in Figure 1.

Hydrogen-Enhanced Decohesion (HEDE) was introduced by Oriani in 1970 which describes HE as the weakening of metal-to-metal bonds due to the presence of hydrogen atoms between metal atoms [69]. This reduction in bond strength facilitates bond breakage at a crack tip. According to this model, a single hydrogen atom can significantly promote crack propagation by jumping from a recently broken bond to a neighboring intact one [71]. On the other hand, hydrogen works as a shield in the interactions among dislocations and, dislocations and other discontinuities in the HELP mechanism [72]. Therefore, the repulsion decreases and dislocations can draw nearer to one another [73]. It facilitates the movement of dislocations in a stress concentration zone, resulting in dislocation pile-up and premature material failure. In this mechanism, the plasticity of the alloy plays a major role in hydrogen-assisted fracture [72].

Lynch et al. [74] proposed the mechanism of AIDE. The basis of this theory is that dislocations form at a stress concentration region and can easily migrate away when subjected to external stress.

When hydrogen is adsorbed and accumulated in such a region, it weakens interatomic bonds, facilitating the initial stages of dislocation and void formation in conjunction with the HELP mechanism [9,75]. Lynch et al. [74] originally used the concept introduced by Clum [76] which focused on the effect of hydrogen on the surfaces and interfaces within the material. The concept is based on the idea that hydrogen adsorption on the metal surface, as observed through field ion microscopy, alters various energy parameters such as surface energy and stacking-fault energy. These energy adjustments are believed to lead to a reduction in the critical shear stress required for the generation of dislocation loops. Consequently, this easing of the nucleation process aids in the formation of dislocations. The analysis of Lynch et al. [74] of the hydrogen influence on dislocation formation contrasts with the hypothesis suggested by Nagumo [77], which proposes the HESIV mechanism, shifting focus from the immediate effects of hydrogen to the indirect damage and material degradation it causes. This hypothesis, proposed by Nagumo and further elaborated in subsequent studies [78], asserts that deformation-induced vacancies, augmented and stabilized by hydrogen, are essential to HE. Observations from various studies highlight the initiation of voids by hydrogen vacancies, particularly at slip bands or cell walls [65,66]. Nagumo [77] suggests that these vacancy clusters are chiefly responsible for the reduced crack growth resistance. However, this model overlooks certain experimental observations such as the increased dislocation velocity and strain rate dependence, which cannot be fully explained solely by the role of vacancies.

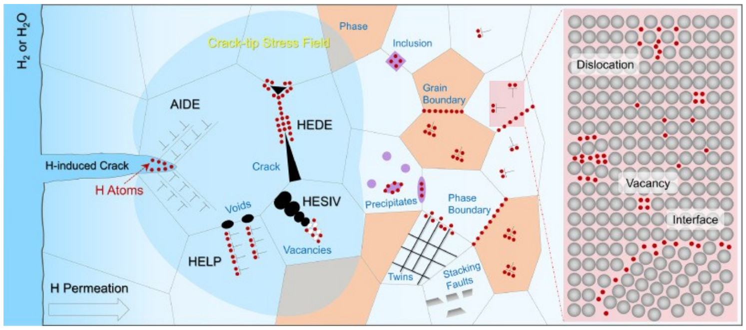

Figure 1. Schematic of hydrogen embrittlement mechanisms [79]

In this section, it was shown that hydrogen influences the atomic structure of steel and therefore, the mechanical and potentially the physical behavior of steel. To fully understand the effects and their extent, studying the effects of hydrogen on steel electron structure is crucial.

2-4 Effect of hydrogen on the electronic structure of steel

In the previous section, the mechanisms of HE were briefly examined. An alternative approach to explain HE is considering the relationship between the atomic and electronic structures of steel, especially in the presence of hydrogen. HE mechanisms consist of analyzing the changes in the electron structure caused by hydrogen in steel in this approach. The results of such changes can be reflected in the physical properties of the material such as electrical resistivity.

The addition of hydrogen with a single electron to the metallic lattice has the potential to cause changes to the electron structure. That can be associated with the bonds of the parent metal. Krasko and Olson [80] used first-principles methods to investigate the impact of hydrogen interstitials on the electron structure of grain boundaries. It was found that hydrogen at grain boundaries has minimal impact on the electron charge in the iron valence d-bands. The hydrogen atoms create a weak covalent bond due to the hybridization of the s-pd orbitals within and across the grain boundary. This bond is located far below the Fermi energy and is not significant in altering the electronic structure of the iron atoms at the grain boundary. These discoveries are essential for comprehending the decohesion mechanisms that can cause hydrogen embrittlement in iron-based alloys.

The change to electronic structure can expand to other discontinuities such as dislocations. Teus et al. [59] noted that the impact of hydrogen interstitials on dislocation mobility could be better understood by considering electron structure alongside the HELP mechanism, therefore an electronic approach to the HELP mechanism was proposed. The analysis of the shear modulus (μ) by Teus et al. [59] revealed that hydrogen reduces its magnitude compared to hydrogen-free FCC γ-Fe. The reduced shear modulus caused by hydrogen lowers the required stress to activate dislocation sources (σ), the line tension of dislocations (Γ), and the distance between dislocations in the pile-ups (d) as shown in Eq. 3, Eq. 4 and Eq. 5, where b is the Burgers vector, L is the distance between pinned points, υ is the Poisson's ratio of the material, $\Re$ is the radius of the dislocation curve and n is the number of dislocations. As a result, the greater mobility of dislocations observed in hydrogen-containing austenite suggests a softening effect attributed to the electron structure altered by hydrogen [81,82]. Due to the smaller radius of hydrogen compared to other common interstitials in iron, it results in lower binding energy to immobile dislocations and causes minor lattice distortions. However, hydrogen can increase dislocation mobility by affecting the electron structure of the host metal. It attracts electrons from iron, significantly increasing the density of states at the Fermi level and therefore the local conduction electron density around dislocations. This effect weakens the Fe-Fe bonds in the lattice [59], thereby enhancing dislocation mobility [83]. The increase in dislocation mobility, along with a decrease in shear modulus, ultimately influences the mechanical behavior of the material.

$$\sigma = 2\pi b/L \qquad \text{Eq. 3}$$

$$\Gamma = (\mu b^2/4\pi)/\log\left(\frac{\mathfrak{R}}{5b}\right) \qquad \text{Eq. 4}$$

$$\mathrm{d} = (\pi b \mu)/16(1-\upsilon)n\sigma \qquad \text{Eq. 5}$$

Using first-principles calculations on BCC iron, Teus et al. [84] demonstrated that hydrogen increases both the density of states at the Fermi level and the concentration of free electrons. This finding was corroborated by Mössbauer spectroscopy results, which indicated that hydrogen enhances interatomic bonds between atoms of the parent metal by increasing the density of states [84]. This increase enhances the metallic character of the bonds, which, unlike covalent bonds, tends to increase plasticity by promoting the initiation and mobility of dislocations rather than contributing to brittleness [85]. Furthermore, electron paramagnetic resonance spectroscopy results showed that increasing hydrogen concentration in austenitic steel leads to electron exchange with the s and d bands of the parent metal, further enhancing the metallic bonds [59,84,86].

To sum, hydrogen influences the electronic structure of steel, affecting the mechanical and physical properties. One such property is electrical resistivity, which can potentially serve as a foundation of a non-destructive testing (NDT) method to detect hydrogen and predict damage before component degradation occurs. The effect of hydrogen on the electrical resistivity of steel is investigated in the next section.

2-6 Resistivity of steel in the presence of hydrogen

2-6-1 Classic and quantum mechanics approach

Both classical and quantum mechanical approaches are required to clarify the impact of hydrogen on the electrical resistivity of steel. In the classical approach, electrons can be viewed as having particle-like characteristics. In this scenario, their interactions are envisioned through elastic collisions with lattice atoms. This notion qualitatively explains the rise in resistivity with an increasing presence of lattice imperfections and alloying elements [34,87]. Hummel [34] explained that the drift velocity of electrons, caused by an external electric field, increases their random motion. As electrons accelerate, the drift velocity increases until they collide with another particle and lose some or all of this velocity. A more accurate model describes electron motion as being opposed by friction. In this point of view, electrons continue to accelerate against the electrostatic force until they reach a final drift velocity, where the forces from the electric field and friction are balanced [34]. As can be observed in Eq. 6 and according to the classical approach, the conductivity of the material σ, is proportional to the number of free electrons N_f, and the time taken between two consecutive collisions known as relaxation time τ, which increases as the mean free path of electrons increases. The electron mass and charge are represented as m and e respectively [34].

$$\sigma = \frac{\mathrm{N}_f \, e^2 \, \tau}{m} \qquad \text{Eq. 6}$$

The classical method has limitations for certain conditions, such as considering that all electrons are available for conduction and simplifying the scattering mechanisms [34]. In quantum mechanics, electrons have wave-like properties where matter waves interact with lattice atoms and scatter in all directions. When waves encounter atoms, they absorb and reemit energy as spherical waves. In a periodic crystal structure, these reemitted waves are in phase in the forward direction, causing constructive interference and resulting in no change in the intensity or direction of the wave, known as coherent scattering. If the atoms are not periodically arranged because of impurities, vacancies, grain boundaries, or thermal vibrations, the scattered waves lose their fixed phase relationship, leading to incoherent scattering and reduced energy in the forward direction [34,88].

When subjected to an external field, the conduction electrons move through an array of ions, and the resistivity is dictated by the rate at which they scatter from an initial state k to a final state k′. k-space is a defined hypothetical space, where k and k′ are vectors defined on the Fermi surface. The Fermi surface represents a constant energy level of electrons in k-space with well-defined boundaries. Only electrons within a certain energy range around the Fermi surface can increase their energy slightly under the influence of an external field [88].

$$\sigma = \frac{1}{3} e^2 v_f^2 \tau \mathrm{N(E)} \qquad \text{Eq. 7}$$

The quantum mechanical Eq. 7 reveals that conductivity is influenced by the Fermi velocity v_f, relaxation time τ, and population density $\mathrm{N(E)}$. The latter, is directly proportional to the density of states. Eq. 7 holds more significance than the expression derived from classical electron theory, Eq. 6. Specifically, the equation highlights that not all free electrons N_f contribute to conduction; rather, conductivity in metals is largely influenced by the population density of electrons near the Fermi surface. For instance, metals such as copper and silver possess partially filled valence bands, leading to high electron population densities near their Fermi energy, and resulting in significant conductivity according to Eq. 7 [34]. The research done by Teus et al. [59] using Density Functional Theory (DFT) confirms these results. This is consistent with the reports of Shivanyuk [85] regarding the enhancement of the metallic character of the bonds of the parent metal in the presence of hydrogen [84,86]. Pontini et al. [89] measured the stacking fault energy change in the presence of hydrogen in AISI 304 steel and reported that the increase in the electrons at the Fermi level leads to a decrease in the stacking fault energy which can lead to dislocations splitting. The rise in electron density at the fermi level and in the vicinity of hydrogen atoms further supports the notion of hydrogen-induced augmentation of conduction electron density in sites occupied by hydrogen atoms. This increase is attributed to various mechanisms, including differences in atom size, valences, and electron concentrations, which affect electron scattering [81]. However, this is a localized impact and resistivity typically increases with higher solute content in the material, with solutes having different effects [82]. According to Brown [91], the resistivity of grain boundaries also depends on the resistivity of the individual dislocations that make up these boundaries. Upon the scattering of electrons that hit the grain boundary, there is a scattering resonance at or close to the Fermi level. It is expected that the presence of hydrogen alters the quantity of scattering and the energy of electrons.

The defects have a certain trapping capacity for hydrogen which makes each microstructure unique when it comes to hydrogen permeation. Elements such as Mo and Ti which are visibly higher in 300M compared to 4340, according to Table 2 in Chapter 3, form carbides that can affect electron scattering. Due to the variations in the type and amount of carbides, the extent of the hydrogen effect on the electron structure of the parent metal differs in each steel alloy.

The abovementioned studies investigated the theoretical and indirect effect of hydrogen on the electron structure of Fe-based alloys. On the other hand, some researchers have used experiments to measure the physical properties that change in hydrogen presence. Mastuo et al. [92] measured the electrical resistivity of Fe-Cr-Al foils charged with high-pressure hydrogen gas and reported no significant change in the resistivity caused by hydrogen. Researchers have published data on the measurement of various physical properties and the effect of hydrogen content, such as the speed of acoustic waves [19], and some endeavors have been made to develop a technique for examining hydrogen levels by observing how these parameters shift in response to fluctuations in hydrogen content; such as measuring the thermoelectric effect [93] and electrical resistivity [17,22].

Ooijen and Fast [43] investigated the effect of hydrogen on the resistivity of pure iron wires and measured the resistivity changes in hydrogen-charged, annealed, and cold-worked wires. The increase in the resistivity of annealed specimens surpassed that of the cold-worked. The primary reason that cold-worked specimens do not show a higher increase in resistivity has been attributed to the alignment and shape of the cracks, which are less disruptive to the electric current flow compared to the more randomly oriented cracks in annealed specimens. Hydrogen precipitated at the crystal boundaries caused high gas pressures, leading to microscopic cracks at the grain boundaries in the cold-worked wires. Additionally, the resistivity increase was attributed to plastic deformation of the metal near the microcavities rather than interstitially dissolved hydrogen [43]. These results highlight the substantial impact of preferred orientation and hydrogen-induced plastic deformation on the electrical resistivity of iron. It underscores the importance of distinguishing between the impact of hydrogen on electron structure and microstructure, since hydrogen can modify both. Raczysnki et al. [94] and Moriya et al. [95] reported contradicting results, stating that hydrogen can lead to an increase in electrical resistivity of armco and zone-melted iron even in the absence of structural damage [94,95]. The recovery of resistivity was examined by measuring the change in the electrical resistivity after hydrogen desorption. Raczysnki et al. [94] reported a recovery close to 100%. Moriya et al. [95] measured the recovery for two sets of iron specimens. The set charged in the less severe conditions of the basic solution had a recovery close to 100%. However, the specimens charged in acidic solution with more severe conditions were not fully recovered in terms of resistivity. The reason is the microstructural permanent damages of steel due to high fugacity hydrogen charging. It is important to note that, these measurements were carried out partially below 50 K to prevent hydrogen desorption and to isolate the increase in resistivity due to lattice vibrations [94,95].

Alternatively, indirect measurements of resistivity appear to conflict with the earlier investigations [59,96] which suggested that the hydrogen dissolved in the interstitial spaces of the alloy increases the number of free electrons, which can potentially lower its electrical resistivity, due to providing more electrons available for conduction and enhancing the metallic properties. However, experimental studies did not conclusively determine the extent to which interstitial solute hydrogen contributed to this change in the electronic structure of the alloy. The effects of solute and irreversibly trapped hydrogen have not been isolated from each other. Developing a method to distinguish between the two would be valuable. Various experimental methods were employed to investigate the impact of hydrogen presence on the electrical properties of iron-based metals. Among these are the four-probe method [16] and the eddy current method [17,22]. These approaches provide valuable insights into how the presence of hydrogen affects the electrical behavior of steel alloys.

In studies employing impedance measurement methods, Koenig et al. [17] and Lasseigne [21] analyzed the electromagnetic behavior of X80 pipeline steel and steel welds. They developed a unique approach to establish a correlation between the hydrogen content and resistivity. Lasseigne claimed that the contribution of inductive reactance (X) was negligibly low at 100 Hz and therefore, the resistance (R) has a linear relation with impedance (Z), according to Eq. 8.

$$Z^2 = R^2 + X^2 \qquad \text{Eq. 8}$$

Subsequently, they observed a rise in the electrical resistance of X80 pipeline steel with an increase in hydrogen concentration, as determined by the eddy current technique as shown in Figure 2. Similarly, Zhou et al. [16] investigated the change in an eddy current signal in a 2.25Cr-1Mo-0.25V due to hydrogen charging. The investigation revealed an increase in the intensity of the signal with increasing charging time and therefore, hydrogen content. Charging time was also correlated with hydrogen-induced plasticity loss. Then, as shown in Figure 3, the loss of plasticity was related to the signal intensity. In a similar study, Zhou et al. [18] reported an increase in the electrical resistivity of low-carbon steel using a four-probe method as well as an impedance measurement procedure. However, the precise mechanism underlying the change in electrical properties due to hydrogen remains unclear in these investigations [16]. Conversely, Bellemare et al. [22] found no discernible change in the electrical conductivity of chromium-plated 4340 steel caused by hydrogen, as assessed via the eddy current method. A cumulative hydrogen content of 1400 atomic ppm was absorbed into both the Cr coating and the martensitic steel substrate during the plating process, of which 430 atomic ppm (approximately 8 weight ppm) was absorbed by the substrate in the latter study.

Yet, even though both studies [22,16] reported a similar hydrogen content of 8 wt ppm, Koenig et al. [17] have observed a rise in the electrical resistivity of X80 pipeline steel using the eddy current method. However, the potential reasons for the observations were not mentioned. Therefore, it is essential to conduct further investigations into the influence of hydrogen on the electrical resistivity of Fe-based alloys. A thorough comprehension of the fundamental physics driving this phenomenon is essential for interpreting the outcomes of these NDT techniques. While the change in resistivity due to irreversible damage induced by hydrogen is evident, the involvement of interstitial hydrogen demands further study.

In this research, the changes of electrical resistivity to hydrogen charging in 4340 and 300M steels were investigated using the four-probe method. The basis of the method and the related studies are discussed in the next section.

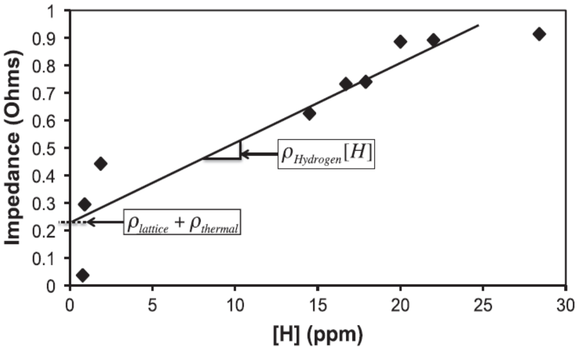

Figure 2. Change in impedance as a function of hydrogen content [17]

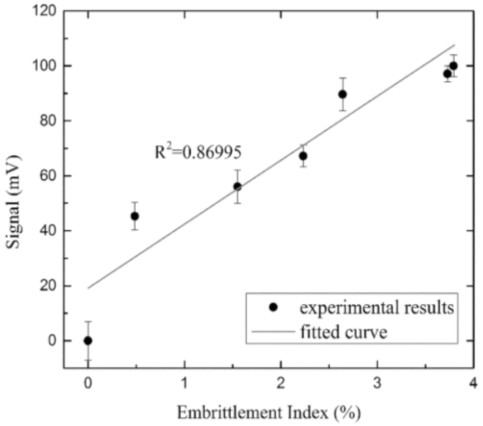

Figure 3. Changes in eddy current signal and embrittlement index [16]

2-6-2 Four-probe method for resistivity measurement

Various techniques have been employed to measure the electrical resistivity of steels. Methods such as Kelvin’s [97] and the four-probe method [98] were commonly utilized. Additionally, researchers have employed the eddy current method to study resistivity [17,21]. Matula et al. [99] employed this method in steady-state utilizing direct current (DC) for measurements. Bowler et al. [98] utilized both AC and DC in four-probe method measurements [100]to measure the potential resistivity drop in ferrous and non-ferrous components. Plate thickness, magnetic permeability, and electrical conductivity were calculated using the measured data. A frequency sweep is required to measure magnetic permeability by this method. For resistivity evaluations, measurements in a single frequency are enough as long as the specimen dimensions are specified [100].

The four-probe method was first used in geophysics in 1916 by Wenner. In 1950s, Valdes applied this method to measure resistivity in semiconductor wafers [101], while Van der Pauw employed it for measuring the potential drop of specimens with arbitrary shapes and metallic bars [102,103]. Currently, the four-probe method is known as a precise technique, used to calibrate setups according to standards. This technique is originally derived from the two-point probe method which may be simpler to implement but lacks the precision offered by the four-probe method [101]. Figure 4. (a) illustrates a schematic of the two-point probe. The two contacts serve to carry both voltage and current. Ohm's law is employed to measure the resistance of the Device Under Test (DUT).

$$\mathrm{R_T} = \frac{\mathrm{V}}{\mathrm{I}} = 2\mathrm{R_W} + 2\mathrm{R_C} + \mathrm{R_{DUT}} \qquad \text{Eq. 9}$$

The total resistance (R_T) in the circuit, as depicted in Eq. 9, is influenced by the resistance of each contact point (Rc) and the resistance of the wire (Rw). By eliminating the contact resistance, one can induce two additional probes and use the voltage probe to record the potential drop. Using two probes introduces complexity in measuring these two contacts. Therefore, two additional contact points are introduced, as illustrated in Figure 4 (b). It is worth noting that the contact surfaces where the probe touches the specimen are required to be small to prevent additional contact resistance. Rc and Rw remain, however, their impact is minimized by the negligible current flow in the inner circuit, due to the high impedance of the voltmeter. Consequently, the voltage drop recorded by the voltmeter accurately reflects the behavior of the DUT [101]. This voltage is recorded in time and resistivity can be calculated accordingly.

In the four-probe method, the probes are positioned linearly, spaced apart by s_1, s_2, and s_3 distances. In a specific scenario where all probe distances are equal to s, and the voltage is measured at a radius s away from the probe, the resistivity can be calculated using Eq. 10 [101].

$$\rho = 2\pi s F \frac{V}{I} \qquad \text{Eq. 11}$$

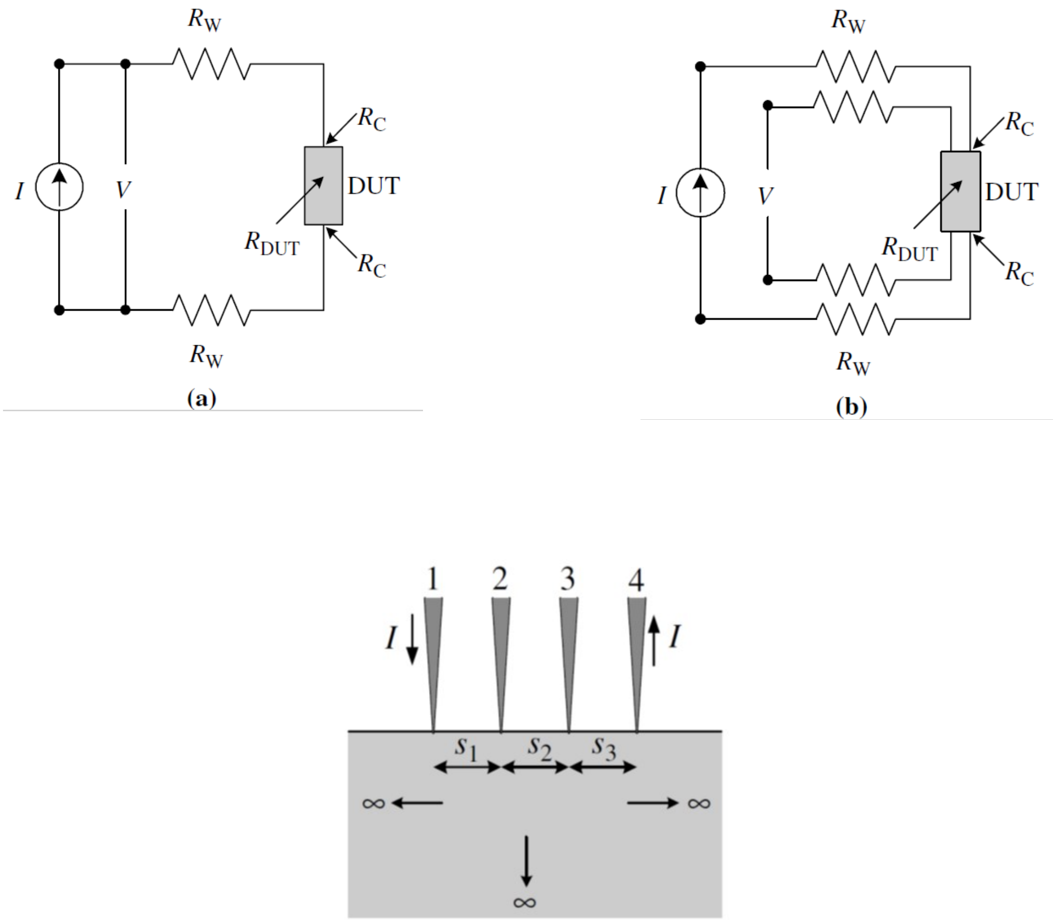

Figure 4. (a) Two-probe method and, (b) four-probe method and resistances, (c) four-point probe showing probe distances and current flow [101]

Voltage is measured in volts, current in amperes, and distance in centimetres. The specimen is assumed to be semi-infinite in Eq. 10. However, if this assumption is not satisfied, correction factors are employed to account for geometric variations. The correction factor (F) is the multiplication of F1, F2, and F3, which correspond to adjustments for sample thickness, dimensions, and probe position relative to the edges of the sample [101].

As outlined by the free electron model [104], the resistivity of conductive materials correlates with the effective mass of electrons, electron concentration, and the primary scattering mechanism. The available literature on the direct measurement of resistivity change caused by hydrogen using the four-probe method is confined to the research done by Zhou et al. [18]. They [18] attempted to quantify the resistivity of steel and its alterations attributed to diffusive hydrogen using the four-probe method. However, they did not outline the potential reasons for the phenomenon. The results of the measured resistivity change using the four-probe method, with the percentage change in hydrogen content, are depicted in Figure 5. As can be seen, an increase is observed in resistivity due to a rise in hydrogen content. The rise in resistivity can be attributed to the scattering effect created by the presence of hydrogen which was explained based on the classical theory of resistivity in the previous sections.

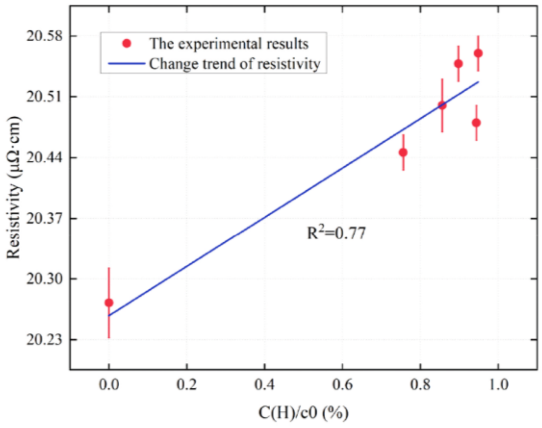

Figure 5. The correlation between resistivity and hydrogen content [18]

As discussed earlier in this chapter, resistivity is primarily governed by the scattering of electrons by lattice and alloying atoms in steel. This predominant scattering mechanism is influenced by factors such as sample composition, structure, temperature, inclusions, and strain. As per

Matthiessen's rule, depicted in Eq. 12, the overall resistivity of a conducting material comprises the intrinsic resistivity of the lattice and additional residual resistivity resulting from various scattering mechanisms caused by hydrogen and temperature [105].

$$\rho = \sum \rho_i = \rho_{lattice} + \rho_{thermal}(T) + \rho_{hydrogen}(H) \qquad \text{Eq. 12}$$

The findings indicate a nearly linear rise in the resistivity as the hydrogen content increases [24]. With longer hydrogen charging durations, there is a notable increase in hydrogen diffusion within the interior of the material. Hydrogen atoms tend to accumulate at grain boundaries, internal flaws, and inclusions to form hydrogen molecules under tensile stress, and consequently, impacting the mechanical characteristics of the material [60]. The extent of hydrogen-induced damage in metallic materials with varying hydrogen levels can be evaluated through performance metrics derived from tensile, impact toughness, and bending tests. Among these, certain mechanical properties exhibit higher sensitivity to changes in hydrogen damage, notably area reduction and elongation [18]. Exploring the interplay between the electron structure of materials and the impact of hydrogen as a particle offers a promising avenue for uncovering insights into the HE of steel components. At present, a notable gap exists in experimental data and theoretical calculations regarding the effect of hydrogen on electron structure, a key factor in embrittlement phenomena.

To address this gap in the present study resistivity measurements have been conducted using the four-probe method for the reasons discussed above. The forthcoming chapters detail the experimental procedures, results, and subsequent discussions. These findings hold potential for developing an NDT method capable of quantifying hydrogen content in iron-based materials using physical properties. This research investigates the ability of the four-probe method to detect changes in resistivity caused by hydrogen in martensitic high-strength medium-carbon steel (4340 and 300M) with the tempered martensitic microstructure.

2-7 Objectives

The main goal of the present research is to investigate the changes in the amount of electrical resistivity of 4340 and 300M as a result of changes in hydrogen content and to evaluate the sensitivity of the methods employed. The specific objectives are as follows:

1- Evaluation of change in electrical resistivity of martensitic 4340 and 300M and the resolution of the effect of hydrogen on it using the four-probe method.
2- Establish a correlation between the extent of variation in electrical resistivity and the hydrogen content.
3- Isolating the effect of hydrogen on electron structure from its effect on microstructure and the manifestation of the two on electrical resistivity.
4- Investigating the factors that impact the contribution of hydrogen to the changes in resistivity, including hydrogen trapping in the two steels affected by alloying elements, microstructural characteristics, and heat treatment. These influences manifest through cracks, hydrogen content, and the effect of desorption on resistivity.

Chapter 3: EXPERIMENTAL PROCEDURES

3-1 Steel sample materials and preparation

The selected materials for the study were high-strength low alloy 4340 and 300M steels with the composition shown in Table 2. Specimens with an average thickness of 0.97 cm were cut from as-received bars with a diameter of 1.27 cm. The temperature and procedure for heat treatment and oil quenching of the 4340 cut specimens were carried out per ASTM F519 standard specifications. The 4340 specimens underwent heat treatment at 825°C for one hour followed by oil quenching. Subsequently, they were tempered at 230°C twice for two hours each [55]. Similarly, the 300M specimens were heat treated at 870°C and oil quenched, followed by a double temper at 300°C. This heat treatment regime aligns with the AMS 6257E standard [70], which is used for aerospace landing gears [106]. The resulting microstructures are shown in Figure 6. The specimens underwent polishing with sandpaper ranging from 60 to 600 grit, followed by pad polishing using a diamond slurry of 6 µm. The final specimen thickness was 0.9 mm. It is important to note that without the final diamond polishing to get a mirror surface, the change in resistivity due to hydrogen charging is not detectable. The possible reasons are discussed in the next chapter.

Table 2. Chemical composition of 4340 and 300M steels (wt %)

Element / Steel	C	Si	Ni	Mn	Cr	Mo	Cu	S	P	V	Ti	Al	Sn
4340	0.39	0.25	1.69	0.73	0.73	0.207	0.250	0.001	0.013	-	-	0.007	-
300M	0.42	1.68	1.89	0.74	0.80	0.40	0.09	<0.001	0.005	0.08	0.0010	0.03	0.006

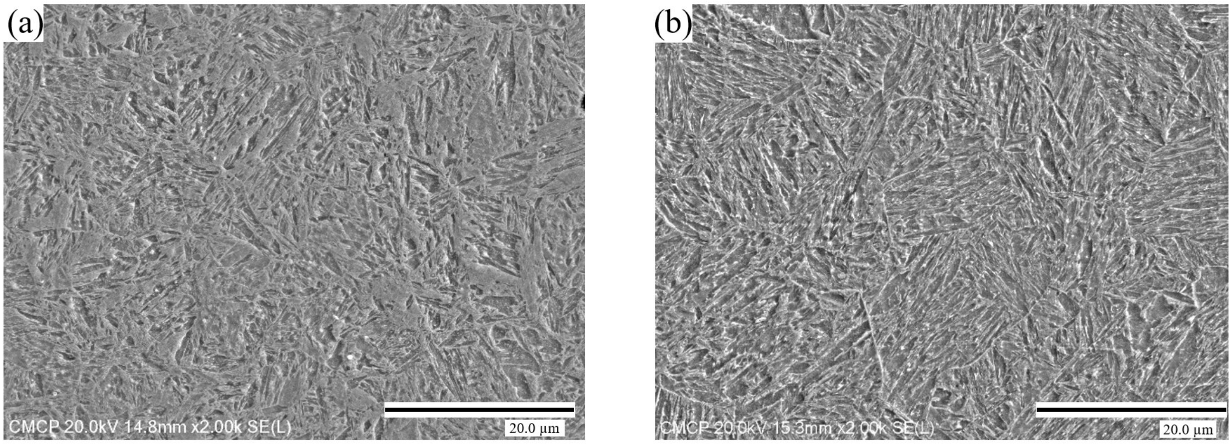

Figure 6. SEM images of final martensitic microstructures of (a) 4340 and (b) 300M, used in this research 20.0 µm

3-2 Electrochemical hydrogen charging

The introduction of hydrogen atoms into the steel can be achieved using methods described in section 2-1 Hydrogen absorption and diffusion in steel. In this study, hydrogen was introduced using the cathodic charging technique, as shown in Figure 7.

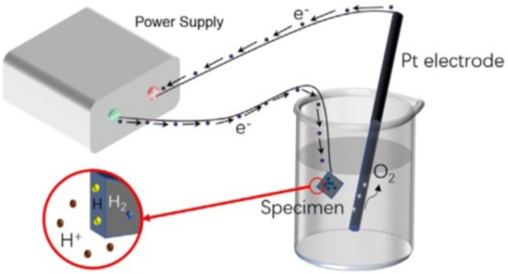

Figure 7. Schematic of electrochemical cathodic charging [107]

Out of the various methods for introducing bulk material with hydrogen, cathodic charging was identified as most practical due to its ease of application and readily accessible setup. Moreover, the electric potential applied during cathodic charging enhances the diffusivity of hydrogen, thereby enhancing the effectiveness of charging when compared to methods solely driven by concentration [32]. In the cathodic cell, hydrogen ions undergo reduction, forming either gas or atomic hydrogen which then gets absorbed onto the surface of the specimen, leading to hydrogen atom diffusion into the metal. This process is achieved using a single-cell setup, with a platinum electrode serving as the anode and the specimen as the cathode. The choice of solution can vary between acidic or basic. An acidic solution offers a higher concentration of hydrogen ions, thereby increasing the fugacity of hydrogen on the surface of the specimen [33].

Ammonium Thiocyanate, NH_4SCN was used as a poison to prohibit the recombination of hydrogen atoms to produce hydrogen gas and prevent the reduction of hydrogen atoms available for diffusion [42]. The amount of poison varies in research reports depending on the targeted hydrogen content and specimen composition. Ando and Yamakawa [108] found that the addition of sulfur, cyanide, and arsenic accelerates hydrogen entry by increasing the coverage of adsorbed hydrogen atoms on the metal surface. However, NH_4SCN was selected for this study due to its ease of handling and safety, while also providing the necessary kinetics required for the process. This choice is supported by the observed reduction in charging time and the resulting hydrogen content [109,110].

Cathodic charging was employed to introduce hydrogen into the material via both radial and surface pathways. The charging parameters were selected to establish a severe hydrogen charging environment, with a current density of 100 mA/cm^2 in constant current mode. The cathodic charging current density was chosen according to the literature to minimize corrosion during hydrogen charging. The charging solution consisted of 0.5M H_2SO_4, with 3 g/l NH_4SCN [111] and a 0.1M H_2SO_4 without the poison. The independent variable was time, which resulted in varying hydrogen content in specimens subjected to similar charging conditions. Each specimen is charged using 250 mL of the prepared solution. A frame made of silver-plated copper wire wrap served as a holder and the current carrier for the specimen. The specimen was connected to the positive pole, while a platinum electrode was connected to the negative pole of the power supply as in Figure 7. After cathodic charging was done and before the start of resistivity measurements, the specimens underwent a gentle polishing using the cloth pad for 6 µm slurry, to eliminate any charging residues and restore their metallic conductivity. Subsequently, they were washed with acetone to remove any contaminations that may interfere with the electrical current.

3-3 Resistivity measurement using the Four-probe method (DC)

The four-probe method was selected due to its precise measurement capabilities and scientifically validated repeatability. The apparatus consists of four gold-plated spring-loaded steel probes mounted on a pillar, which is lowered onto the specimen using a lever. The two outer probes are connected to the TTi PL303-P power supply, as seen in Figure 9 (a) showing the entire setup. The inner probes are connected to the Keithley 2182A nanovoltmeter. Voltage measurements were taken at 800, 600, 400, and 200 mA in constant current mode for each specimen before and after hydrogen charging. A Python script was used to record voltages through an RS232 port, generating voltage-time graphs. The accuracy of the method was assessed using a standard resistor, and the measurement resolution was in nanovolts. The voltage data was acquired as a function of time, as in Figure 8. The resistivity was calculated using Eq. 10 in chapter 2, where a constant current was applied from the power supply, and the voltage was measured using the nanovoltmeter.

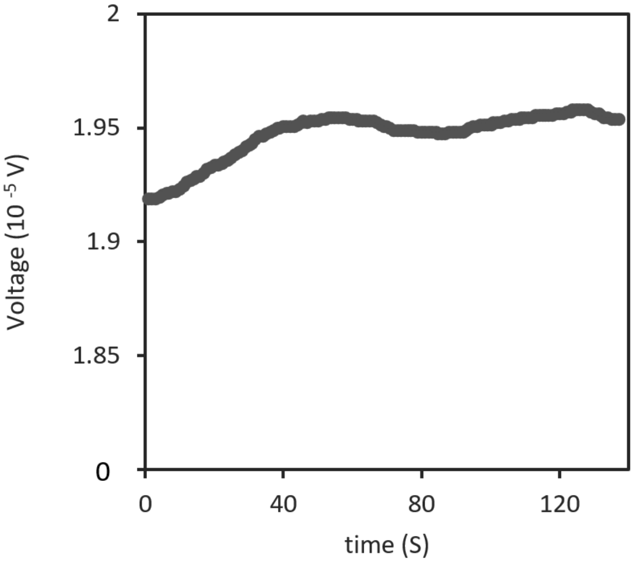

Figure 8. Raw data showing voltage-time graph for a non-charged 4340 specimen measured at 200mA

3-4 Hydrogen content measurement

The specimens utilized for measuring hydrogen content were cut from identical 4340 and 300M bars. Their thickness was standardized to 1mm to ensure the precision of the hydrogen content measurement using the hydrogen analyzer apparatus. Three separate experiments for hydrogen content were conducted for each charging duration per material. After cutting specimens from steel bars, the specimens underwent heat treatment following the industry standard. After oil quenching and tempering, each specimen went through grinding and polishing before being subjected to hydrogen charging. After the charging process, the specimens underwent minimal polishing to restore the surface conditions to improve the accuracy of the resistivity measurements. Subsequently, the specimens were cleansed with acetone, dried, and immediately introduced into the hydrogen analyzer, which was calibrated using standard specimens. The employed analyzer is an Eltra H-500 gas analyzer model by ATS Scientific INC shown in Figure 9 (b) Once calibration was completed with the standard steel balls provided by Eltra, the specimen under study was placed in a quartz boat and lowered into the heated section of the furnace, maintained under a nitrogen atmosphere at a constant temperature of 1000°C. The gas desorbed from the specimen is conveyed using nitrogen gas to the filters and detectors, with the quantity of hydrogen reported in weight parts per million (wt ppm).

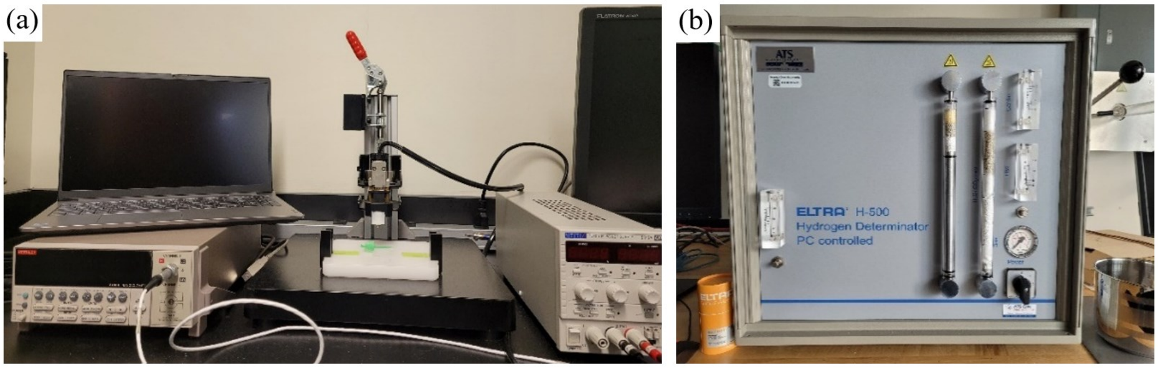

Figure 9. (a) The resistivity measurement setup and (b) hydrogen content analyzer

3-5 Characterization

Uncharged specimens of 4340 and 300M were prepared for SEM imaging, EDS and EBSD using sandpaper with additional steps of polishing up to 1200 grit, followed by pad polishing using a diamond slurry of 6, 3, and 1 μm. EBSD specimens were ion-milled for 15 minutes before analysis using a Hitachi IM400II apparatus. To prepare hydrogen-charged specimens for SEM imaging, the samples were polished using only a polishing pad and 1 μm diamond slurry.

Chapter 4: RESULTS AND DISCUSSION

This chapter provides an in-depth examination and explanation of the resistivity measurement findings, demonstrating the impact of hydrogen on the electrical resistivity of 4340 and 300M.

Initially, the degree to which electrical resistivity was affected by hydrogen in the two materials is evaluated using the four-probe method. Following that, an investigation into potential explanations associated with the observations is undertaken. Moreover, the discussion examines the degree to which variations in electrical resistivity are affected by microstructural changes and irreversible damage, as opposed to being solely attributed to solute hydrogen.

4-1 Effect of hydrogen on the electrical resistivity of 4340 and 300M

Figure 10 depicts a voltage-current graph for 4340 steel measured using the four-probe method. The measurement was done before and after hydrogen charging carried out in a 0.5 M H_2SO_4 solution containing 3 g/l NH_4SCN at a current density of 100 mA/cm^2. Although this method is sensitive to the changes in resistivity due to hydrogen, it seems that surface conditions play an important role in the detection of any changes. The alteration in resistivity becomes measurable only on specimens polished to a mirror surface finish. This observation shows the criticality of flawless probe contact, particularly at microscales. A measurement for 200 seconds was done for each material and charging condition. The results of measurement done on each current, are fitted using linear regression, as shown in Figure 10. The linearity conforms with a coefficient of determination ranging from 0.96 to 0.99 for all measurements. The linearity indicates that the measurement aligns with Ohm's law, as demonstrated in Eq. 13 with the slope increasing after hydrogen charging. Figure 11 shows the electrical resistivity of 4340 and 300M as a function of charging time in a 0.5M H_2SO_4 solution containing 3 g/l NH_4SCN. For the resistivity measurements, the current was adjusted from 200 mA to 800 mA while the voltage was recorded using the voltmeter in parallel with the probes. The resistivity was calculated for each current, and the reported value represents the average of these measurements. Each data point on the graph represents the average of three resistivity measurements conducted under identical conditions. The zero charging has a small error bar showing that the local microstructural changes from specimen to specimen do not affect the resistivity measurements. Both steels exhibit a significant increase in resistivity at the start, accelerating by the second hour and approaching saturation after 7 hours of charging.

$$R = V/I \qquad \text{Eq. 13}$$

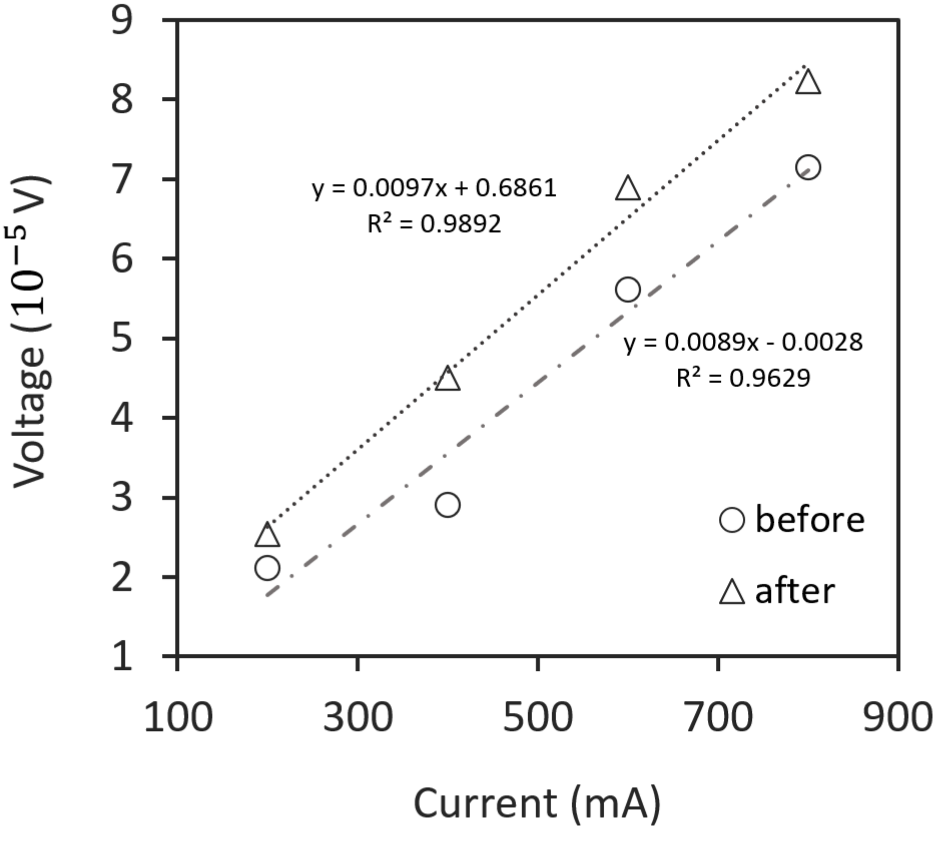

Figure 10. Voltage - Current graph for a 4340 specimen before and after hydrogen charging in 0.5 M H_2SO_4 containing NH_4SCN, at the current density of 100 mA/cm^2

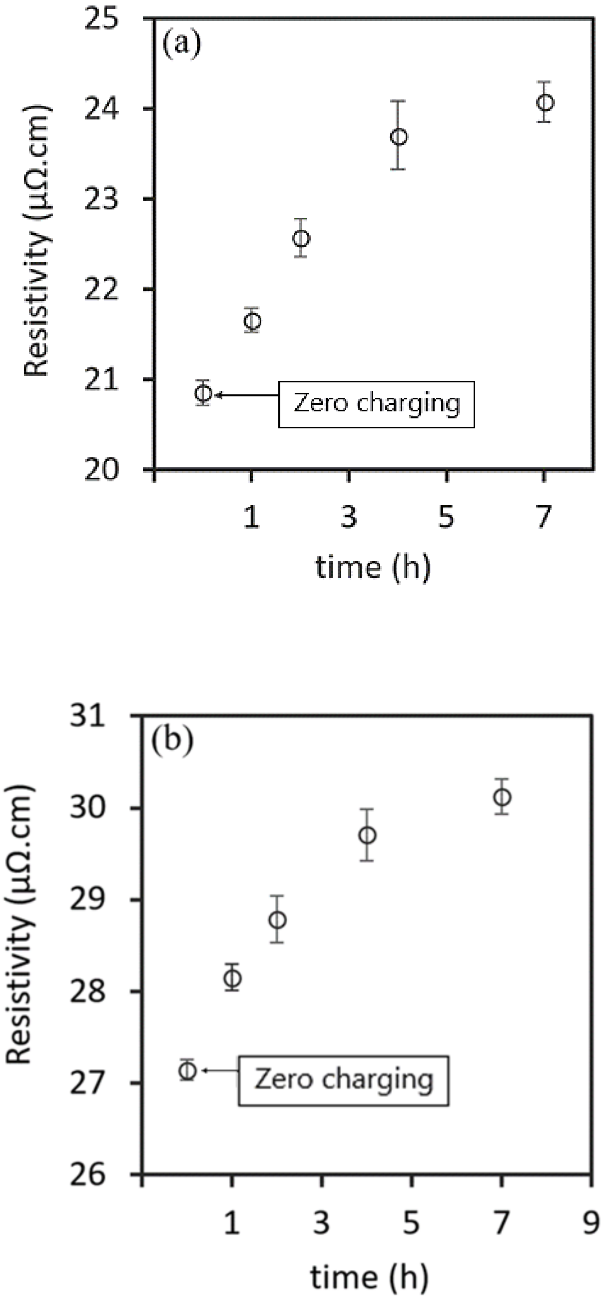

Figure 11. Change in resistivity as a function of charging time for (a) 4340 and (b) 300M, hydrogen charged in 0.5 M H_2SO_4 containing 3 g/l NH_4SCN, at the current density of 100 mA/cm^2

In Figure 12, the percentage change in resistivity of steels is compared, revealing that the change in resistivity for both alloys after 1 hour of charging is nearly identical. The formula used to calculate the percentage change in resistivity is as per Eq. 14; where, ρ_{charged} and ρ_0 are the resistivities of charged and uncharged specimens, respectively. The percentage increase in the resistivity of 4340 is 3.7, 8.9, 14.0 and 15.3 % for 1, 2, 4, and 7 hours of charging, respectively. However, 300M shows a comparatively moderate increase in resistivity, stabilizing after 4 hours of charging, which indicates saturation. Both alloys begin to reach saturation after 4 hours of charging. The change in 300M's resistivity is 4.7, 6.0, 7.0 and 8.8 % for 1 to 7 hours of charging. The smaller change in resistivity in 300M compared to 4340 may be due to its different microstructural features and composition, which will be discussed in the next section.

$$\text{\% change in resistivity} = \left(\frac{\rho_{\text{charged}} - \rho_0}{\rho_0}\right) \times 100 \qquad \text{Eq. 15}$$

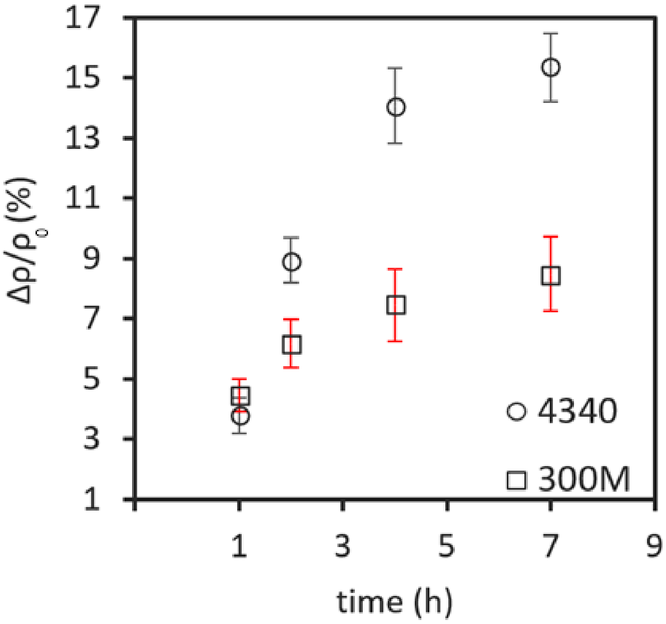

Figure 12. Percentage change in resistivity with charging time for 4340 and 300M, hydrogen charged in 0.5 M H_2SO_4 containing 3 g/l NH_4SCN, at the current density of 100 mA/cm^2

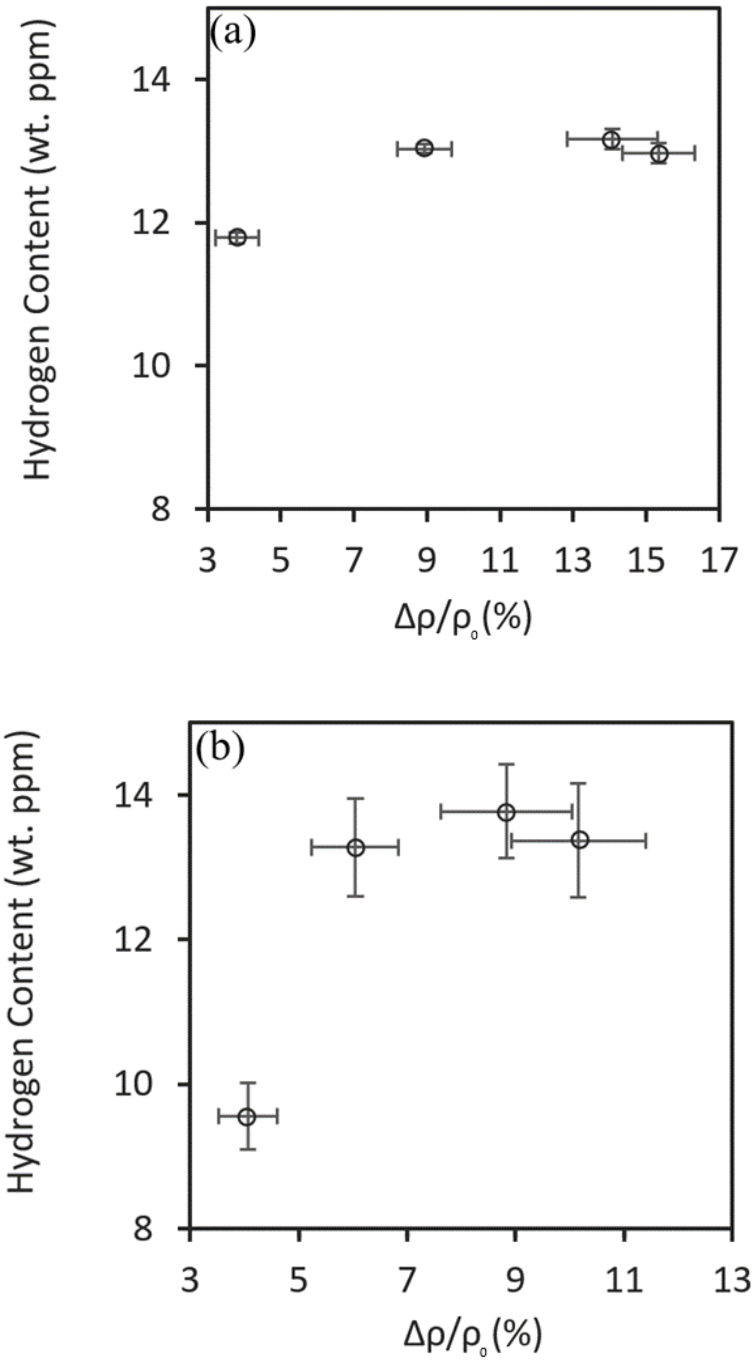

Figure 13. Percentage change in resistivity as a function of hydrogen content for (a) 4340 and (b) 300M hydrogen charged in 0.5 M H_2SO_4 containing 3 g/l NH_4SCN, at the current density of 100 mA/cm^2

The percentage change in resistivity for 4340 and 300M with the change in hydrogen content is shown in Figure 13. It is evident that the hydrogen content of 4340 remains nearly constant after the first hour of charging. Although the percentage change in resistivity is nearly the same in both alloys in the first hour of charging, 300M exhibits a significantly lower hydrogen content during the first hour of charging as compared to 4340. However, after 4 hours of charging, the hydrogen content in both alloys becomes nearly identical. After one hour of charging, a significant amount of hydrogen was detected. Extending the charging time from 1 to 7 hours did not notably increase the hydrogen amount but did enhance resistivity in both alloys. The initial increase in resistivity can be attributed to the hydrogen-induced change in the electron structure of steel [18], while the later increase can be due to the damage made to the steel structure by hydrogen [43]. Damages can manifest in microcracks, which appeared on 4340 after 4 hours of charging, whereas in 300M they appeared after 2 hours.

Overall, hydrogen influences electrical resistivity by altering the electron structure, with its effects also manifesting in the microstructure of the material. The following section examines the extent of these microstructural changes in the studied steels and their correlation with resistivity.

4-2 The multifaceted effects of hydrogen

4-2-1 The impact of microstructure and composition on hydrogen-induced change in electrical resistivity of 4340 and 300M

As evident from Figure 11 in the last section, the resistivity of 4340 is lower in the uncharged condition as well as the charged condition as compared to that of 300M. This can be attributed to the microstructural differences of the two steel alloys. Both microstructures of 4340 and 300M are comprised of martensite laths. Microstructures were investigated using EBSD in pre-charging conditions. The martensite grain morphology is similar in both steels. The results shown in Figure

14 and Figure 15 confirm the hierarchical microstructural features. The grain structure consists of martensite laths, which form blocks. These blocks group into packets, which are contained within prior austenite grains, and both packets and grains vary in length. A block is composed of numerous laths that share almost identical crystallographic orientations, while a packet contains several blocks with nearly the same planes. A prior austenite grain refers to a region that corresponds to a single grain in the austenite state. The block boundaries display irregular shapes, vary in size, and exhibit high levels of misorientation (10º < h < 60º), as illustrated in Figure 14 (c). A large fraction of the boundaries in these figures are high angles. Although the average grain sizes in 4340 and 300M are similar, 19 and 20 μm, the blocks of 300M are thinner and more intricate than 4340 according to Figure 6 (Section 3-1 Steel sample materials and preparation), and Figure 15. As shown in Figure 14, a considerable number of blocks in 4340 are oriented in (100) and (111) planes respectively for cementite and martensite. For 300M these orientations are (101) and (010) respectively as shown in Figure 15. A certain fraction of grains exhibit orientations that result in varied atomic packing along specific crystallographic directions. Therefore, the orientation, and the fine texture of blocks in 300M, can result in a higher resistivity than 4340 in the pre-charged condition. The secondary effects of this texture and its influence on after-charging diffusivity will be discussed in the following discussion.

After 4 hours of hydrogen charging, blister wall cracks appeared on 4340 steel as shown in

Figure 16. On the other hand, fine cracks were prevalent in the 300M specimens after 2 hours of charging as shown in Figure 17, indicating that damage developed more quickly and severely in 300M than in 4340 steel. Irreversibly trapped hydrogen atoms at precipitates and their interfaces are likely more abundant in 300M, as indicated by its lower hydrogen diffusion coefficient

compared to 4340 [54]. This irreversibly trapped hydrogen can be the original cause of the microstructural damage and the slower rise in electrical resistivity after hydrogen charging in 300M compared to 4340. The hydrogen near trap sites is expected to affect resistivity less than the solute hydrogen. Although hydrogen hinders electron transmission, its impact on resistivity is masked when trapped.

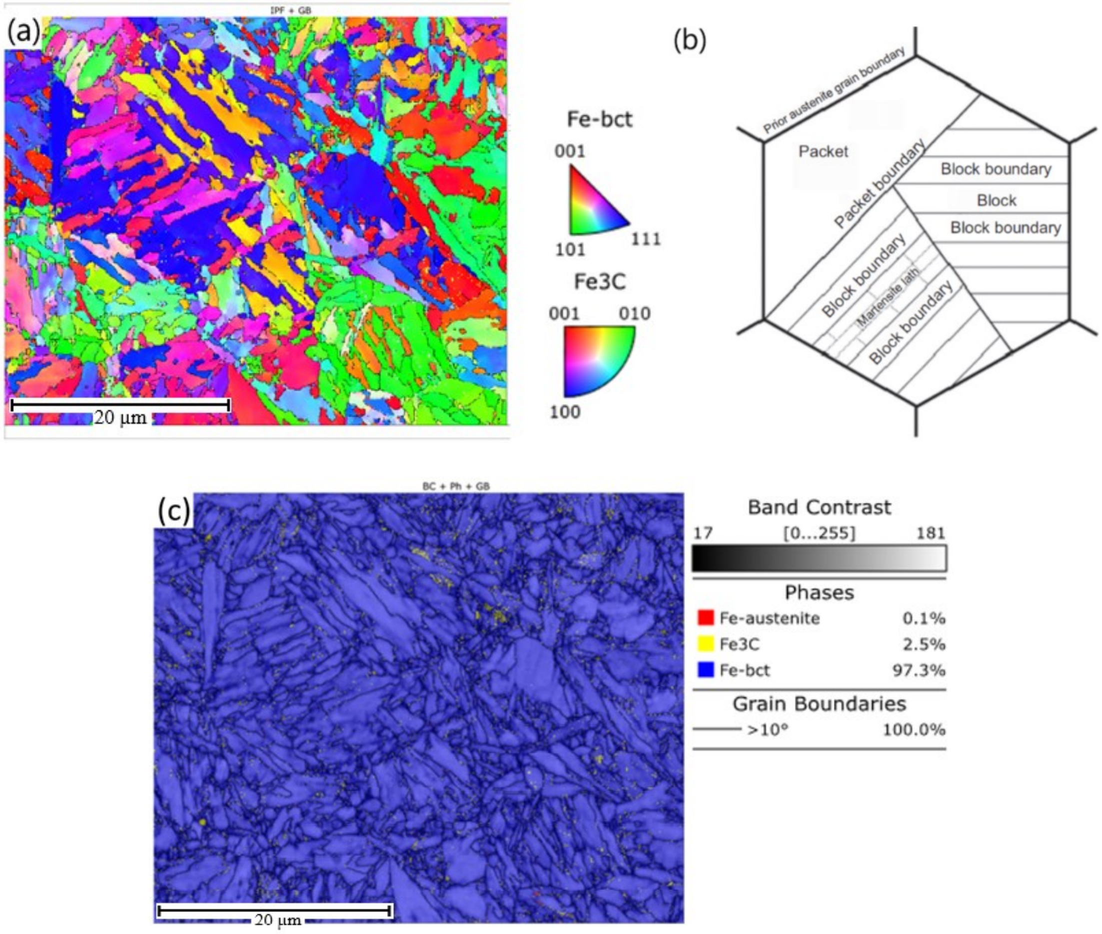

Figure 14. (a) The EBSD and the inverse pole figure map (IPF-Z) of martensitic 4340 operated at 25 kV parallel to the Z direction shows grain boundaries and martensite lath blocks. The stereographic triangles for BCT and Fe_3C are shown (b) Hierarchy in a martensitic microstructure [112]. (c) The EBSD map showing the Austenite and cementite at the lath boundaries of non-charged 4340

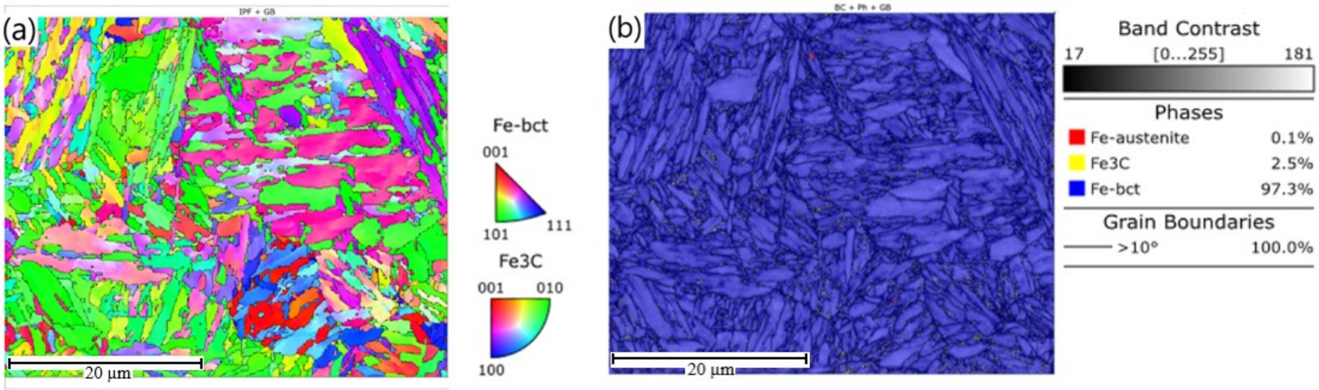

Figure 15. The EBSD and the inverse pole figure map (IPF-Z) of martensitic 300M operated at 25 kV parallel to Z direction. The stereographic triangles for BCT and Fe_3C. (b) Austenite and cementite at the lath boundaries of non-charged 300M

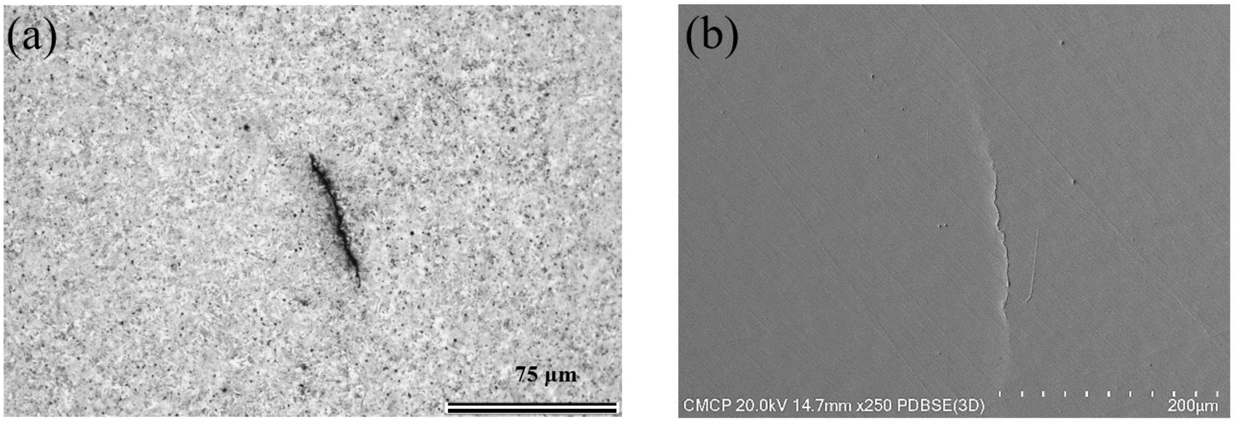

Figure 16. A blister wall crack in 4340, hydrogen charged for 4 hours in 0.5 M H_2SO_4 containing 3 g/l NH_4SCN, at the current density of 100 mA/cm^2. (a) OM image, (b) SEM image

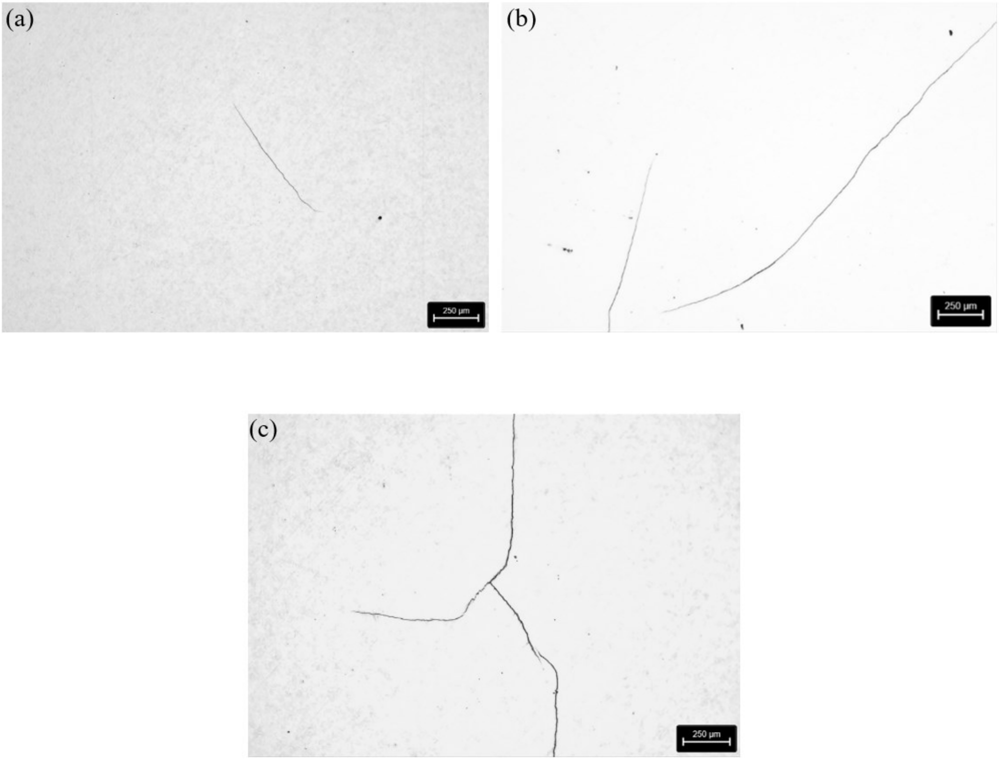

Figure 17. Optical microscopic images of 300M charged for (a) 2, (b) 4 and (c) 7 hours, in a 0.5 M H_2SO_4 solution containing 3 g/l NH_4SCN, at the current density of 100 mA/cm^2

The significance of precipitates in hydrogen trapping and subsequent cracking lies in their capacity to contain substantial quantities of hydrogen, thereby influencing the energies of vacancies and dislocations [71]. The formation of precipitates in 4340 and 300M is expected to be different depending upon the composition and heat treatment. As can be seen in Figure 14, the amount of Fe_3C in 300M is comparatively lower than that of 4340. The silicon content in 300M surpasses that of 4340 steel (Table 2), which can contribute to the stabilization of ε-carbides which have a higher trapping capacity than cementite [58]. The higher nickel content in 300M results in a more retained austenite-to-ferrite ratio, which can alter hydrogen distribution by being an effective trap.

Figure 18 and Figure 19 illustrate the potential presence of copper-containing precipitates in combination with oxygen and sulfur across and along the cracks in hydrogen-charged 4340 charged in 0.5 M H_2SO_4 containing 3 g/l NH_4SCN, at the current density of 100 mA/cm^2. These elements were detected at various locations along the cracks in the steel and they can act as damage initiation points during hydrogen charging. A prevailing theory suggests that hydrogen induces expansion at microstructural interfaces within steel due to internal pressures, raising the possibility of hydrogen existing in molecular form within the material.[113]. Monoatomic hydrogen absorbed into the lattice recombines to make hydrogen gas at internal structural discontinuities such as the ones discussed above. The resultant elevated pressure induces the expansion of microcracks and microvoids, ultimately leading to their coalescence. This mechanism effectively accounts for the formation of numerous voids and irreversible damage such as hydrogen-induced cracking in the absence of external stress and can happen as a result of high fugacity charging [113]. However, increasing the number of effective trapping sites for diffusible hydrogen has been used to increase the resistance of martensitic steels against hydrogen embrittlement. Lin et al. [62] utilized copper (Cu) precipitates to achieve this objective; effectively impeding hydrogen diffusion within the steel matrix. Their research highlights a substantial improvement in hydrogen trapping capacity through copper precipitation, which offers stronger trapping sites than dislocations, with an activation energy of 35.6 kJ mol^{-1}. However, it is reported that the precipitation of copper particles potentially increases stress accumulation at the interface of precipitate/ martensite laths. In this research, cracks initiated and propagated in regions rich in copper, oxygen and sulfur within specimens subjected to severe charging conditions and contained high levels of hydrogen as seen in Figure 18.

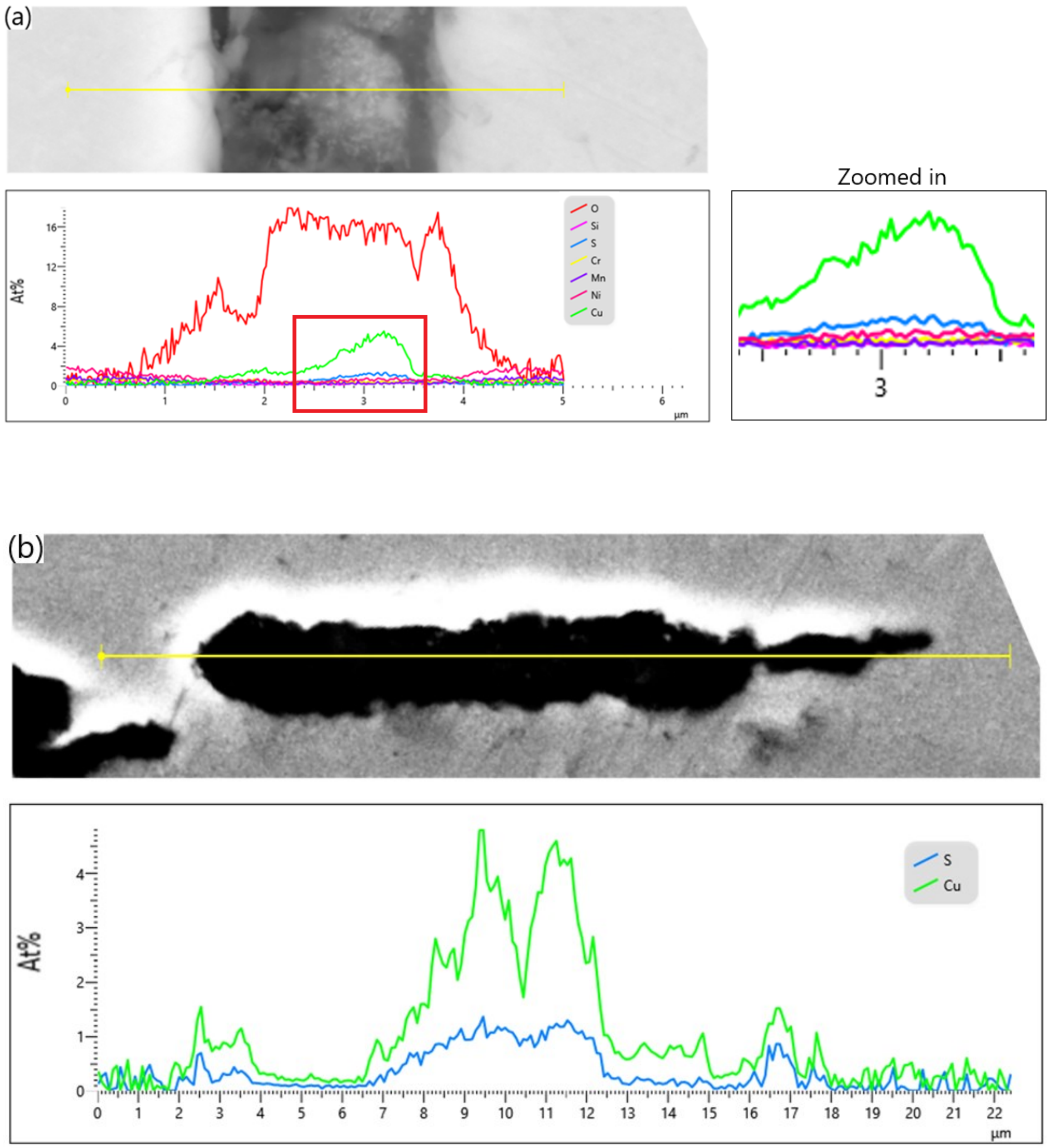

Figure 18. Cu-containing precipitates at crack initiation points in hydrogen-charged 4340 steel(a) across the crack containing oxygen, (b) along the crack containing sulfur

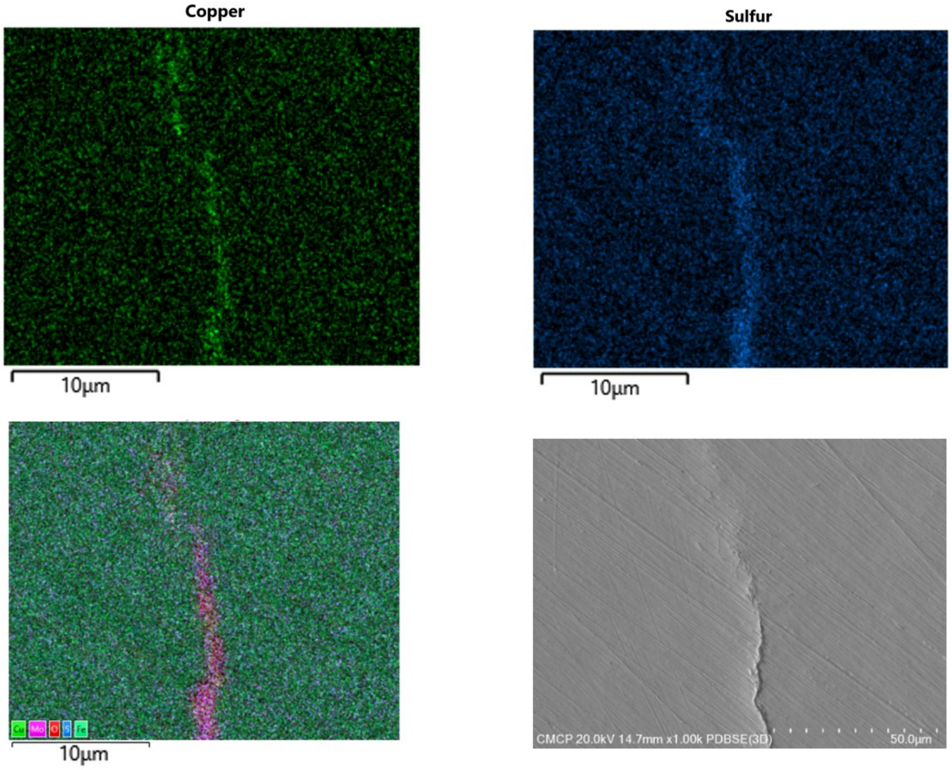

Figure 19. EDS mapping of crack in hydrogen-charged 4340 steel showing copper and sulfur concentrations along the crack opening.

On the other hand, 300M steel contains less copper and more aluminum as compared to 4340 as shown in Table 2. A cracked aluminum oxide particle was observed in the microstructure of the charged 300M specimen as seen in Figure 20 (a). Deep cracks observed on the surface of 300M steel, can originate from the aluminum oxide particles in their vicinity as in Figure 20 (b). Dislocations that form around the Al_2O_3 inclusion act as hydrogen traps [114]. Moreover, using ab initio modelling, Hüter et al. [115] showed that aluminum can hinder the movement of hydrogen atoms in steel and reduce their diffusivity by trapping them. In this study, Al_2O_3 was not observed directly along the crack path. However, another potential cause for crack formation, aside from brittle inclusions, could be the presence of preferred orientations that are more susceptible to cracking.

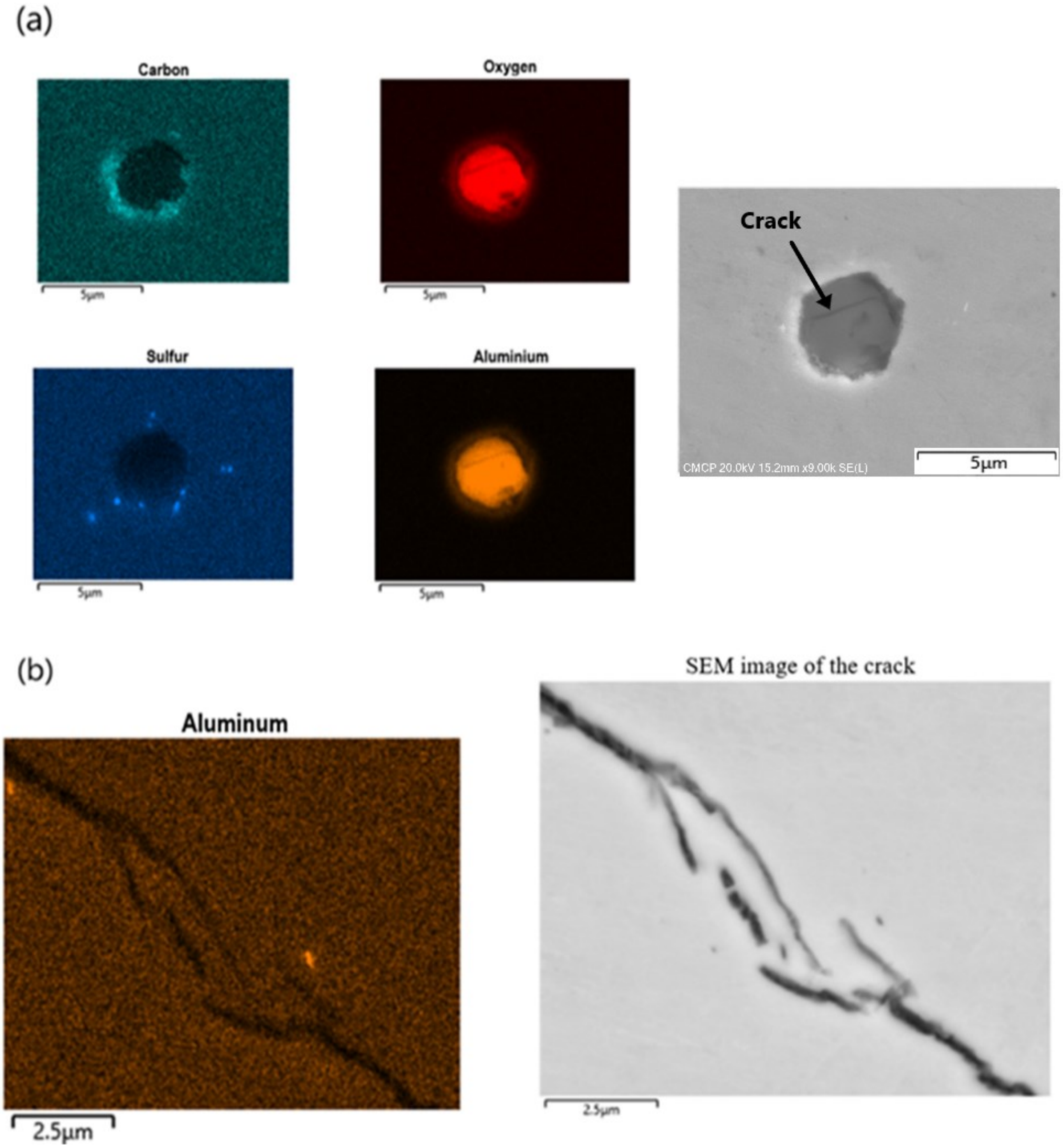

Figure 20. (a) Cracked inclusion primarily composed of Al and O in 300M steel, highlighting a potential crack initiation site due to its composition, (b) Aluminum-rich precipitate located close to a crack in 300M steel.

Apart from precipitates, it is reported that certain planes and orientations can contribute to blister and crack formation when subjected to hydrogen charging. Microstructural analysis revealed that transgranular hydrogen environment-assisted cracking occurs along the martensite blocks of $\{110\}_{BCT}$ plane [116]. However, this plane acts as both a trans-block slip plane, continuous across a packet, and a plane parallel to the block interface [117]. Despite this, experiments confirmed that hydrogen cracking propagates along block/lath boundaries [118]. Specifically, hydrogen enhances dislocation movement along $\{110\}_{BCT}$ slip planes within a packet, redistributing hydrogen to the intersected martensite block and packet boundaries [118]. Lath interfaces within the grains serve as effective hydrogen traps. The cumulative quantity of hydrogen trapped in these interfaces can exceed the amount trapped in the prior austenitic grain boundaries and inclusions by a factor of 5 to 30 [119].

Hydrogen causes an increase in resistivity with or without the damage caused by the precipitates or facilitated by crystallographic orientations. It is uncertain whether the resistivity can fully return to the uncharged value after hydrogen desorption. To investigate the recoverability of resistivity, the interactions of hydrogen and traps need to be discussed. The hydrogen atoms in the lattice are the diffusible atoms with a low binding energy and are reversibly trapped [120]. Hydrogen is desorbed from such traps at ambient temperature, recovering the resistivity. The recovered amount can be attributed to the changes that hydrogen made to the energies of the conducting band of iron electrons [35]. The remaining unrecovered resistivity has two components: the first is due to the hydrogen being irreversibly trapped, and the other is a result of damage [45]. This can be attributed to hydrogen facilitating the movement of dislocations and vacancy stabilization leading to permanent damage that exhibits surface cracks and blisters [78,118].

The changes observed in resistivity measurements of 4340 and 300M capture the combined effects of solute and irreversibly trapped hydrogen. The next section explores an investigation aimed at distinguishing these effects from one another.

4-2-2 Recovery in resistivity after hydrogen desorption

The electrical resistivity (ρ) of 4340 and 300M specimens were measured before and after hydrogen charging as compared in Figure 12. To isolate the effect of solute hydrogen on the resistivity of subject steels, the charged specimens were placed at ambient temperature and pressure for 24 and 500 hours to measure the percentage recovery in the resistivity of these specimens after the desorption of hydrogen. Percentage recovery is calculated according to Eq. 16. Where, ρ_{desorbed} is the resistivity measured after desorption of hydrogen at ambient temperature.

$$\% \text{ Recovery} = \frac{\rho_{\text{charged}} - \rho_{\text{desorbed}}}{\rho_{\text{charged}} - \rho_{0}} \times 100 \qquad \text{Eq. 16}$$

The results show that resistivity is recovered up to nearly 70% in 4340 and 60% in 300M after 24 hours of desorption. After 500 hours of desorption, percentage recovery in 300M remains unchanged while for 4340 up to 80% recovery is observed as depicted in Figure 21. Since the recovery is below 100 percent, the 4340 and 300M specimens have sustained some permanent damage even after 1 h. The lower recovery of 300M as compared to 4340 is consistent with the potential reasons discussed earlier in Section 4-2-1. The reasons include a greater hydrogen trapping capacity in 300M compared to 4340, along with a higher diffusion coefficient in 4340 relative to 300M. Although surface microcracks did not appear in 4340 steel after 2 hours of charging, the partial recovery of resistivity suggests that hydrogen caused permanent damage.

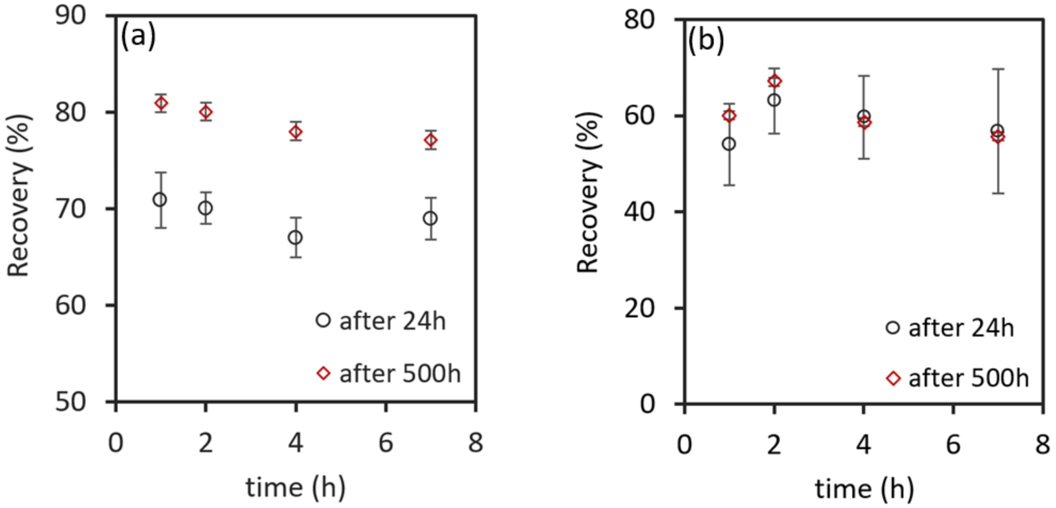

Figure 21. Percentage recovery of resistivity with time for (a) 4340 and (b) 300M hydrogen charged in 0.5 M H_2SO_4 containing 3 g/l NH_4SCN at 100 mA/cm^2

The greater recovery in 4340 is due to reversibly trapped and diffusible hydrogen, which has a larger effect on electrical resistivity compared to the irreversibly trapped hydrogen [45]. 300M has more irreversible traps with higher binding energies. Therefore, the resistivity changes in 300M are influenced more by its microstructural defects, rather than solely by hydrogen.

As discussed the effect of hydrogen on resistivity depends on its trapping location. It also significantly influences electrical resistivity by altering the electron structure. Despite their similar microstructure, the differing behavior in resistivity between the two alloys likely originates from differences in their electron structure. In the early stages of charging, the electrical resistivity in 300M specimens rose similarly to that in 4340, despite lower hydrogen content in 300M. At this stage, hydrogen atoms are primarily trapped in the lattice. However, in later hours, resistivity changes, particularly in 300M, are influenced by microstructural damage. During the resistivity measurement, a direct current passes through the specimen and electrons of the material at the Fermi surface acquire velocity. Electron matter waves scatter off metal ions, dispersing radiation in various directions. Fe ions absorb and reemit energy as spherical waves, while hydrogen, as an impurity, oscillates differently and influences Fe ion vibrations. It alters local force constants, affecting the host lattice. As a result, electron scattering occurs directly via these barriers or indirectly through phonon emission and interference. [121]. The scattering of electrons passing through the specimen can also be affected by hydrogen ions. If electron energy dissipation in the crystal lattice did not occur, electrons at the Fermi level would continuously gain energy, accelerating indefinitely in the applied field. However, since this is not the case, scattering cannot be purely elastic. Electrons can emit or absorb phonons, altering their wavevector and energy. [34,88]. Therefore, in this context, the impact of hydrogen on the electrical resistivity is analogous to that of alloying elements. Furthermore, in the case where the lattice is a transition metal such as iron, ions have a high density of states at the Fermi level which facilitates electron-electron scattering. In this research, the particle nature of hydrogen significantly impacts resistivity. As electrons move through the material, foreign atoms create "friction" with each collision, increasing resistivity [34,88]. Damage caused by severe charging conditions masks the distinction between the two types of trapped hydrogen. Given their differing effects on resistivity, a new set of experiments was designed to explore the possibility of isolating them. The results are presented and discussed in the next section.

4-3 Isolated effect of solute hydrogen on resistivity

As described in the previous sections, cracks appeared on the 300M specimens, affecting their resistivity significantly. However, the change attributed to solute hydrogen was not distinguishable from that caused by damages. In this research, a set of experiments was designed to investigate the effect of solute hydrogen on electrical resistivity. The work of Bellemare [22], demonstrated that

4340 specimens with hydrogen content as high as 8 wt ppm remained un-damaged and showed no change in impedance. In the previous section, significant damage was observed in 300M specimens, therefore 4340 was not chosen for the current tests. 300M specimens were prepared under identical conditions and specifications as those used for 4340. A solution of 0.1 M H_2SO_4 was used to charge specimens at the current density of 100 mA/cm^2. The resistivity of the specimens was measured and change in resistivity was calculated and plotted as presented in Figure 22 to Figure 24. The highest amount of change in resistivity was 4.45%, observed in the specimen with a maximum amount of 0.41 wt ppm hydrogen. As can be seen in Figure 24, the relationship between the hydrogen content and the percentage change in resistivity is linear. Similar results have been obtained by Zhou et al. [18] for the relation of hydrogen content and electrical resistivity in low alloy low carbon steel.

No damage, such as cracks, was observed in these specimens even after 7 hours of charging. The charging condition was milder as a result of lower acidity due to a more dilute solution and also due to the lack of NH_4SCN which prevented the recombination of hydrogen atoms. In the previous experiments in section 4-1 Effect of hydrogen on the electrical resistivity of 4340 and 300M, even after only two hours of charging induced 8 wt ppm of hydrogen leading to damage and changes in the electrical resistivity. The difference in resistivity before and after charging can be attributed to the type of hydrogen trapping influenced by charging conditions. During mild charging, hydrogen was dissolved in interstitial sites and even this small amount made changes to the resistivity. Resistivity recovered close to 100% as no microstructural damage occurred, indicating that the change in resistivity is attributed to diffusible hydrogen. The reversibility and type of hydrogen trapping can be partially evaluated through recovery measurement as shown in Figure 25. The increase in resistivity is almost fully recovered after 24 hours of resting at ambient temperature.

The critical hydrogen content in martensitic steel that causes embrittlement is reported as 0.4 wt ppm [122]. Since the detected amount in this research is close to the critical value, resistivity measurement appears to be a promising method capable of demonstrating the presence of hydrogen.

To conclude, the electrical resistivity of 4340 and 300M increased following electrochemical hydrogen charging, with trapping playing a key role in this effect. Resistivity showed an almost linear increase with hydrogen content, which can be trapped in the lattice and desorbed at ambient temperature. In contrast, irreversibly trapped hydrogen in microstructural defects, such as inclusions, had a smaller impact on resistivity than solute hydrogen. These findings could form the basis for developing an NDT method to detect hydrogen and predict damage before component degradation in the industrial setup.

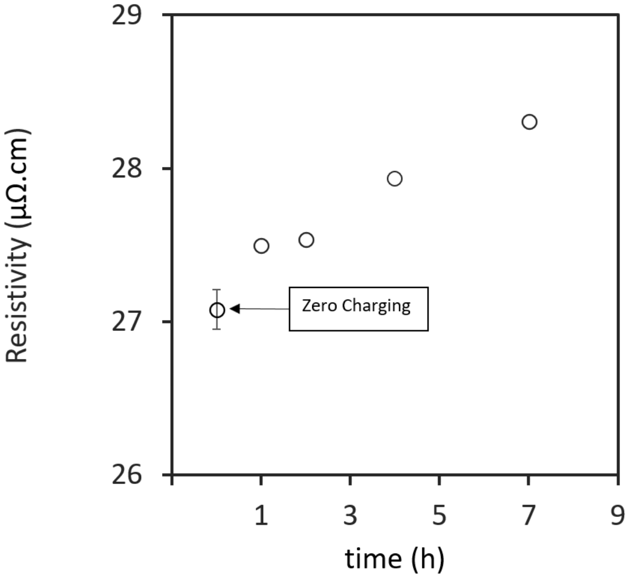

Figure 22. Electrical resistivity of 300M as a function of charging time. Specimens were charged in 0.1 M H_2SO_4 at 100 mA/cm^2

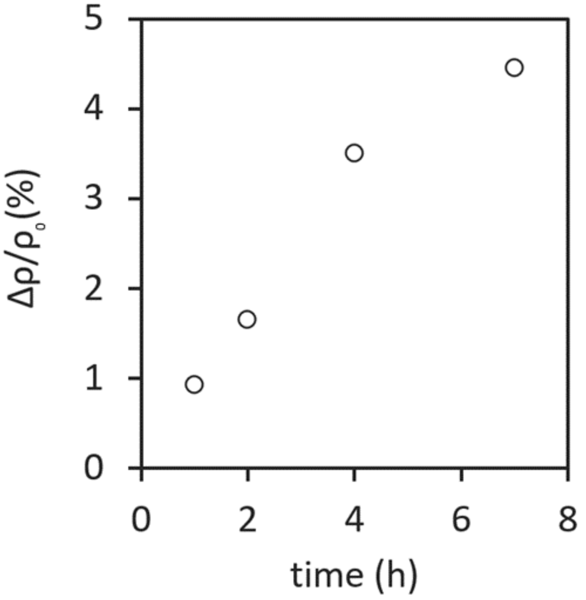

Figure 23. Percentage change in resistivity of 300M as a function of charging time. Specimens were charged in 0.1 M H_2SO_4 at 100 mA/cm^2

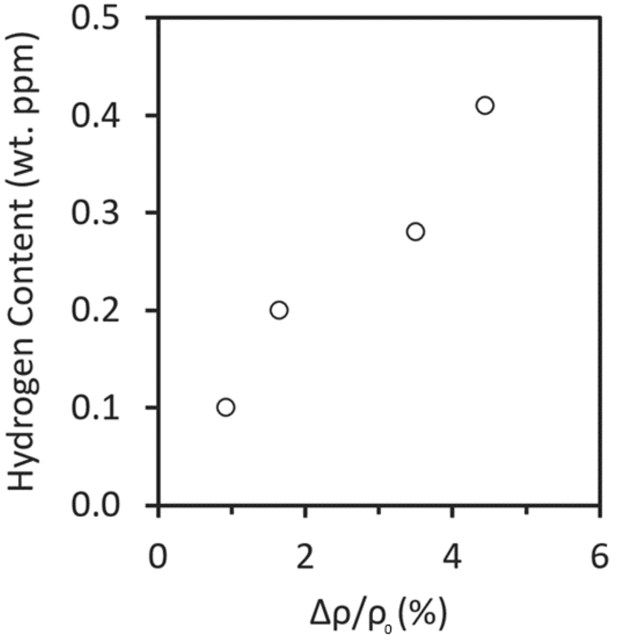

Figure 24. Hydrogen content as a function of percentage change in resistivity for 300M specimens charged in 0.1 M H_2SO_4 at 100 mA/cm^2

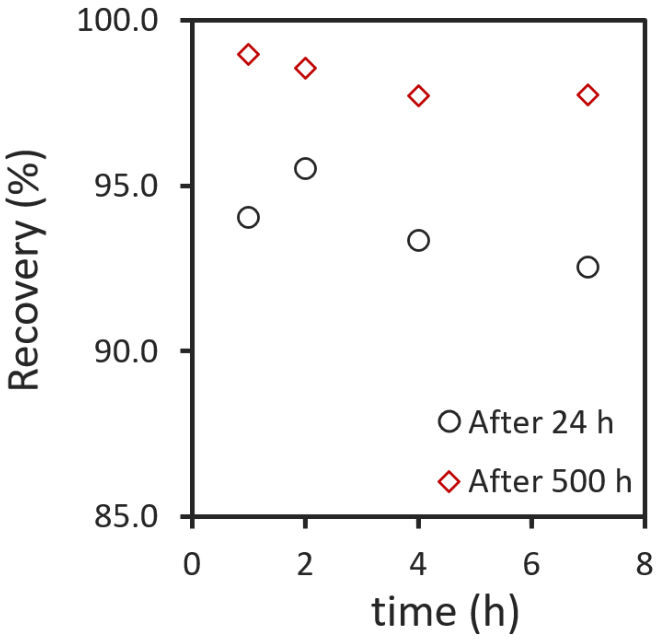

Figure 25. Percentage recovery of resistivity in each charging time for 300M hydrogen charged in 0.1 M H_2SO_4 at 100 mA/cm^2

Chapter 5: CONCLUSIONS

The present study investigates hydrogen-induced changes in electrical resistivity observed in 300M and 4340 low alloy steels utilized in the aerospace industry. Given the susceptibility of these high-strength steels to HE originating from post-manufacturing processes, the detection and assessment of hydrogen content hold considerable significance for aerospace applications. Due to the critical demands of the aerospace sector, this research aims to contribute to the research efforts to develop a non-destructive measurement strategy for detecting hydrogen embrittlement. The findings derived from this investigation are summarized as follows:

1- Electrical resistivity of 4340 and 300M exhibits a notable rise due to an increase in hydrogen content.

2- Interstitial hydrogen plays a major role in changing the electronic structure of the host lattice, directly affecting the electrical resistivity. This insight underscores the importance of understanding the interaction of hydrogen with crystal structure.

3- The hydrogen trapped in discontinuities and defects of the microstructure, causes a smaller amount of change in the resistivity than interstitial hydrogen. Despite this, it can still cause permanent microstructural defects such as cracking.

4- Electrochemically supplied hydrogen can cause cracking, particularly originating near inclusions. This underscores the vulnerability of microstructural imperfections as initiation sites for hydrogen-induced damage.

5- The change in resistivity is highly sensitive to several factors such as the surface conditions of the specimen, alloy composition, and the microstructure.

6- The resistivity increases linearly with hydrogen concentration in the absence of damage.

5-1 Original contributions

This research offered key insights into the sensitivity of electrical resistivity to hydrogen content in 4340 and 300M steels, using the four-probe method. A significant contribution of this thesis is the establishment of a correlation between shifts in electrical resistivity due to hydrogen charging and the specific sites where hydrogen is trapped. Hydrogen retained within the iron lattice alters its electron structure and thus its electrical resistivity, while hydrogen trapped in microstructural defects or near impurities impacts resistivity in a distinct manner. Notably, this approach achieved hydrogen detection at levels as low as 0.40 wt ppm, which is the critical threshold for hydrogen embrittlement in martensitic steels such as 4340 and 300M. These findings deepen the understanding of the interaction of hydrogen with the steel structure and lay a foundation for developing a non-destructive testing method to detect hydrogen embrittlement.

5-2 Future work

Portable four-probe devices are already in use in industry and they can be upgraded to measure the resistivity of components on site. The probe spacing and positioning can be optimized for more precise results. Below are several additional recommendations for future investigations:

1- Utilizing a method to investigate the onset of void formation in the material during electrochemical charging. This approach will aid in discerning the threshold at which hydrogen begins to induce changes in resistivity and initiates damage.

2- Exploring the possibility of amplifying the changes in resistivity at low hydrogen levels by adjusting the probe arrangement, current density, amplifiers, and other factors.

3- Exploring the effect of the contact area of the probes on the accuracy of resistivity measurements.

4- Investigating the effect of hydrogen on the electrical resistivity of materials with different compositions and structures, such as FCC and BCC.

5- Gaining deeper insights into the fundamental physics underlying the experimental results through first-principle calculations.

References

[1] D.K. Singh, R.K. Singh Raman, S.K. Maiti, T.K. Bhandakkar, S. Pal, Investigation of role of alloy microstructure in hydrogen-assisted fracture of AISI 4340 steel using circumferentially notched cylindrical specimens, Mater. Sci. Eng. A 698 (2017) 191–197.

[2] V.G. Gavriljuk, V.M. Shyvaniuk, S.M. Teus, Hydrogen in engineering metallic materials: from atomic-level interactions to mechanical properties, 1st ed, Springer International Publishing, Cham, (2022).

[3] S. Cho, G.I. Kim, S.J. Ko, J.S. Yoo, Y.S. Jung, Y.H. Yoo, J.G. Kim, Comparison of hydrogen embrittlement susceptibility of different types of advanced high-strength steels, Mat. 15 (2022) 3406.

[4] X. Zhu, W. Li, H. Zhao, L. Wang, X. Jin, Hydrogen trapping sites and hydrogen-induced cracking in high strength quenching & partitioning (Q&P) treated steel, Int. J. Hydrog. Energy 39 (2014) 13031–13040.

[5] J. Bellemare, S. Laliberté-Riverin, D. Ménard, M. Brochu, F. Sirois, Subtleties behind hydrogen embrittlement of cadmium-plated 4340 steel revealed by thermal desorption spectroscopy and sustained-load tests, Metall. Mater. Trans. A 51 (2020) 3054–3065.

[6] J. Bellemare, S. Laliberté-Riverin, D. Ménard, Coating density as the key factor behind hydrogen embrittlement of cadmium-plated 4340 steel, J Appl Electrochem 50 (2020) 1045–1058.

[7] V. Singh, R. Singh, K.S. Arora, D.K. Mahajan, Hydrogen induced blister cracking and mechanical failure in X65 pipeline steels, Int. J. Hydrog. Energy 44 (2019) 22039–22049.

[8] R. Singh, A. Singh, P.K. Singh, D.K. Mahajan, Role of prior austenite grain boundaries in short fatigue crack growth in hydrogen charged RPV steel, Int. J. Press. Vessels Pip. 171 (2019) 242–252.

[9] M.B. Djukic, G.M. Bakic, V.S. Zeravcic, A. Sedmak, B. Rajicic, The synergistic action and interplay of hydrogen embrittlement mechanisms in steels and iron: localized plasticity and decohesion, Eng. Fract. Mech. 216 (2019) 106528.

[10] C.D. Beachem, A new model for hydrogen-assisted cracking, Metall. Trans. 3 (1972) 441–455.

[11] G. Chai, T. Antonson, S. Wessman, L. Ryde, Microstructures and hydrogen embrittlement fracture mechanisms in 17-4PH martensitic stainless steel, Procedia Struct. Integr. 42 (2022) 155–162.

[12] A. Świerczyńska, D. Fydrych, M. Landowski, G. Rogalski, J. Łabanowski, Hydrogen embrittlement of X2CrNiMoCuN25-6-3 super duplex stainless steel welded joints under cathodic protection, Constr. Build. Mater. 238 (2020) 117697.

[13] T. Depover, K. Verbeken, The detrimental effect of hydrogen at dislocations on the hydrogen embrittlement susceptibility of Fe-C-X alloys: an experimental proof of the HELP mechanism., Int. J. Hydrog. Energy 43 (2018) 3050-3061.

[14] D.E. Jiang, E.A. Carter, Diffusion of interstitial hydrogen into and through bcc Fe from first principles, Phys. Rev. B 70 (2004) 064102.

[15] L. Vandewalle, M.J. Konstantinović, T. Depover, K. Verbeken, The potential of the internal friction technique to evaluate the role of vacancies and dislocations in the hydrogen embrittlement of steels, Steel Res. Int. 92 (2021) 2100037.

[16] H. Zhou, X. Chi, Q. Wang, H. Pan, J. Chen, Characterization of hydrogen embrittlement in 2.25Cr-1Mo-0.25V steel by eddy current method, Res. Nondestruct. Eval 29 (2018) 212–220.

[17] K. Koenig, A.N. Lasseigne, J.W. Cisler, B. Mishra, R.H. King, D.L. Olson, Non-contact, nondestructive hydrogen and microstructural assessment of steel welds, Int. J. Press. Vessels Pip. 87 (2010) 605–610.

[18] H. Zhou, H. Huang, D. Ye, W. Qiang, C. Zhu, The impact of hydrogen on mechanical performance of carbon alloy plates detected by eddy current method, Nondestruct. Test. Eval. 38 (2023) 683–699.

[19] A.I. Kustov, A.V. Budanov, I.A. Migel, The study of the effect of hydrogen on physical-mechanical properties of steel by acoustic microscopy methods, In: hydrogen materials science and chemistry of metal hydrides. NATO science series, Springer, Netherlands, Dordrecht, (2002) 131–140.

[20] D.L. Olson, Joining of advanced and specialty materials, Proceedings of materials solutions on joining of advanced and specialty materials, Indianapolis, Indiana, (2002) 118–124.

[21] A.N. Lasseigne, Development of thermoelectric power and electromagnetic techniques for determination of interstitials in advanced materials, Doctoral thesis, Colorado School of Mines, Colorado, USA (2006).

[22] J. Bellemare, D. Ménard, F. Sirois, Detection of hydrogen embrittlement in plated high-strength steels with eddy currents: is the sensitivity sufficient?, J. Nondestruct. Eval. 39 (2020) 46.

[23] A.R. Troiano, The role of hydrogen and other interstitials in the mechanical behavior of metals, Metallogr. Microstruct. Anal. 5 (2016) 557–569.

[24] A.N. Lasseigne-Jackson, J.E. Jackson, D.L. Olson, B. Mishra, Development of electromagnetic techniques for hydrogen content assessment in coated linepipe steel, Proceedings of AIP conference, Portland, Oregon 894 (2007) 1159–1166.

[25] T. Das, E. Legrand, S.V. Brahimi, J. Song, S. Yue, Evaluation of material susceptibility to hydrogen embrittlement (HE): an approach based on experimental and finite element (FE) analyses, Eng. Fract. Mech. 224 (2020) 106714.

[26] R.P. Gangloff, B.P Somerday, Gaseous hydrogen embrittlement of materials in energy technologies. The problem, its characterization and effects on particular alloy classes, Woodhead Publishing Ltd (2012) 817-840.

[27] J.S. Kim, Y.H. Lee, D.L. Lee, K.T. Park, C.S. Lee, Microstructural influences on hydrogen delayed fracture of high strength steels, Mater. Sci. Eng. A 505 (2009) 105–110.

[28] Y. Adda, J. Philibert, La diffusion dans les solides, Institute national des sciences et techniques nucléaires, Presses universitaires de France, Saclay, Paris (1966).

[29] M.A.V. Devanathan, Z. Stachurski, W. Beck, A technique for the evaluation of hydrogen embrittlement characteristics of electroplating baths, J. Electrochem. Soc. 110 (1963) 886-890.

[30] J. Woodtli, R. Kieselbach, Damage due to hydrogen embrittlement and stress corrosion cracking, Eng. Fail. Anal. 7 (2000) 427–450.

[31] A. Thomas, J.A. Szpunar, Hydrogen diffusion and trapping in X70 pipeline steel, Int. J. Hydrog. Energy 45 (2020) 2390–2404.

[32] E.E. Fletcher, A.R. Elsea, The effects of high-pressure, high temperature hydrogen on steel, Defence metals information center, Battelle memorial institute, Columbus, Ohio (1964).

[33] N. Ehrlin, C. Bjerken, M. Fisk, Cathodic hydrogen charging of Inconel 718, AIMS Mater. Sci. 3 (2016) 1350–1364.

[34] R.E. Hummel, Electronic properties of materials, 2nd ed., Springer Berlin, Heidelberg, (1985).

[35] R.A. Oriani, The physical and metallurgical aspects of hydrogen in metals, proceedings of the fourth international conference on cold fusion. Fusion Technol. Palo Alto, CA, (1994) 235-266.

[36] R. Cotts, Nuclear magnetic resonance on metal-hydrogen systems, Hydrog. Met. Basic Prop. (2005) 227–265.

[37] C. Marchi, B. Somerday, S. Robinson, Permeability, solubility and diffusivity of hydrogen isotopes in stainless steels at high gas pressures, Int. J. Hydrog. Energy 32 (2007) 100–116.

[38] J.P. Hirth, Effects of hydrogen on the properties of iron and steel, Metall. Trans. A 11 (1980) 861–890.

[39] N. Moody, S. Robinson, W. Garrison, Hydrogen effects on the properties and fracture modes of iron-based alloys, Res. Mech, 30 (1990) 143–206.

[40] J.-Y. Lee, S.M. Lee, Hydrogen trapping phenomena in metals with B.C.C. and F.C.C. crystals structures by the desorption thermal analysis technique, Surf. Coat. Technol. 28 (1986) 301–314.

[41] M. Śmiałowski, Hydrogen in steel: effect of hydrogen on iron and steel during production, fabrication, and use, Pergamon Press ; Wydawnictwa Naukowo-Techniczne, Oxford, New York, (1962).

[42] I.-O. Shim, J.G. Byrne, A study of hydrogen embrittlement in 4340 steel I: mechanical aspects, Mater. Sci. Eng. A 123 (1990) 169–180.

[43] D.J.V. Ooijen, J.D. Fast, Electrical resistance of hydrogen-charged iron wires, Acta Metall. 11 (1963) 211–216.

[44] A. Drexler, T. Depover, S. Leitner, K. Verbeken, W. Ecker, Microstructural based hydrogen diffusion and trapping models applied to Fe–CX alloys, J. Alloys Compd. 826 (2020) 154057.

[45] V.V. Kuznetsov, V.A. Frolov, Determination of the electrical resistivity of metals during electrolytic hydrogen absorption, Zhur. Priklad. Khim. 33 (1960) 628-632.

[46] A. Kholtobina, R. Pippan, L. Romaner, D. Scheiber, W. Ecker, V. Razumovskiy, Hydrogen trapping in BCC iron, Mat. 13 (2020) 2288.

[47] S. Frappart, X. Feaugas, J. Creus, F. Thebault, L. Delattre, H. Marchebois, Hydrogen solubility, diffusivity and trapping in a tempered Fe–C–Cr martensitic steel under various mechanical stress states, Mater. Sci. Eng. A 534 (2012) 384–393.

[48] E. Tal-Gutelmacher, D. Eliezer, E. Abramov, Thermal desorption spectroscopy (TDS)—Application in quantitative study of hydrogen evolution and trapping in crystalline and non-crystalline materials, Mater. Sci. Eng. A 445 (2007) 625–631.

[49] Y. Fukai, Metal-hydrogen system under extended p, T conditions, in: the Metal-hydrogen system: basic bulk properties, Springer Berlin Heidelberg, Berlin, Heidelberg, (1993) 71–119.

[50] S.M. Lee, J.Y. Lee, Trapping and transport phenomena of hydrogen in Nickel, Metall. Trans. Phys. Metall. Mater. Sci. 17 A (1986) 181–187.

[51] D.L. Johnson, J.K. Wu, Hydrogen transport in carbon steels as a function of carbon content and heat treatment near 298 K, J. Mater. Energy Syst. 8 (1987) 402–408.

[52] K. Ebihara, T. Suzudo, H. Kaburaki, K. Takai, S. Takebayashi, Modeling of hydrogen thermal desorption profile of pure iron and eutectoid steel, ISIJ Int. 47 (2007) 1131–1140.

[53] W.Y. Choo, J.Y. Lee, Thermal analysis of trapped hydrogen in pure iron, Metall. Trans. A 13 (1982) 135–140.

[54] D. Figueroa, M.J. Robinson, Hydrogen transport and embrittlement in 300M and AerMet100 ultra high strength steels, Corros. Sci. 52 (2010) 1593–1602.

[55] ASTM F-519-13, Test method for mechanical hydrogen embrittlement evaluation of plating/coating processes and service environments, ASTM International, PA, USA (2017).

[56] A. Drexler, F. Konert, O. Sobol, M. Rhode, J. Domitner, C. Sommitsch, T. Böllinghaus, Enhanced gaseous hydrogen solubility in ferritic and martensitic steels at low temperatures, Int. J. Hydrog. Energy 47 (2022) 39639–39653.

[57] W. Pepperhoff, M. Acet, Constitution and magnetism of iron and its alloys, 1st ed., Springer Berlin Heidelberg, Berlin, Heidelberg, (2001) 147-181.

[58] R.M. Horn, R.O. Ritchie, Mechanisms of tempered martensite embrittlement in low alloy steels, Metall. Trans. A 9 (1978) 1039–1053.

[59] S.M. Teus, V.N. Shivanyuk, B.D. Shanina, V.G. Gavriljuk, Effect of hydrogen on electronic structure of fcc iron in relation to hydrogen embrittlement of austenitic steels, Phys. Status Solidi A 204 (2007) 4249–4258.

[60] D.A. Mirzaev, A.A. Mirzoev, K.Yu. Okishev, A.V. Verkhovykh, Hydrogen–vacancy interaction in bcc iron: ab initio calculations and thermodynamics, Mol. Phys. 112 (2014) 1745–1754.

[61] K. Ohsawa, K. Eguchi, H. Watanabe, M. Yamaguchi, M. Yagi, Configuration and binding energy of multiple hydrogen atoms trapped in monovacancy in bcc transition metals, Phys Rev B 85 (2012) 094102.

[62] Y. L. Liu, Y. Zhang, H. B. Zhou, G. H. Lu, F. Liu, G. N. Luo, Vacancy trapping mechanism for hydrogen bubble formation in metal, Phys Rev B 79 (2009) 172103.

[63] E.J. McEniry, T. Hickel, J. Neugebauer, Atomistic modelling of light-element co-segregation at structural defects in iron, Procedia Struct. Integr. 13 (2018) 1099–1104.

[64] V.P. Ramunni, T.D.P. Coelho, P.E.V. de Miranda, Interaction of hydrogen with the microstructure of low-carbon steel, Mater. Sci. Eng. A 435–436 (2006) 504–514.

[65] T.J. Marrow, M. Aindow, P. Prangnell, M. Strangwood, J.F. Knott, Hydrogen-assisted stable crack growth in iron-3 wt% silicon steel, Acta Mater. 44 (1996) 3125–3140.

[66] F. Terasaki, T. Kawakami, A. Yoshikawa, N. Takano, Terasaki F, Kawakami T, A, Takano, Mechanism of crack propagation due to hydrogen embrittlement in iron single crystals stressed along [001] axis, Rév Métall, 95 (1998) 1519–1529.

[67] W. Zhang, Evaluation of susceptibility to hydrogen embrittlement—A rising step load testing method, Mater. Sci. Appl. 7 (2016) 389–395.

[68] D.M. Allen-Booth, J. Hewitt, A mathematical model describing the effects of micro voids upon the diffusion of hydrogen in iron and steel, Acta Metall. 22 (1974) 171–175.

[69] M.E. Stroe, Hydrogen embrittlement of ferrous materials, Doctoral thesis, Université Libre de Bruxelles, Belgium (2006).

[70] ASTM F1941-00, Standard specification for electrodeposited coatings on threaded fasteners, Unified Inch Screw Threads (UN/UNR), ASTM International, USA (2006).

[71] R. Kirchheim, A. Pundt, Hydrogen in metals, in: physical metallurgy, 5th ed., (2014) 2597–2705.

[72] M. Nagumo, Hydrogen embrittlement: theories, in: encyclopedia of iron, steel and their alloys, 1st ed., (2016) 1785-1800.

[73] D. An, Y. Zhou, Y. Xiao, X. Liu, X. Li, J. Chen, Observation of the hydrogen-dislocation interactions in a high-manganese steel after hydrogen adsorption and desorption, Acta Metall. Sin. Engl. Lett. 36 (2023) 1105–1112.

[74] S. Lynch, Hydrogen embrittlement phenomena and mechanisms, Corros. Rev. 30 (2012) 105–123.

[75] S.K. Dwivedi, M. Vishwakarma, Hydrogen embrittlement in different materials: a review, Int. J. Hydrog. Energy 43 (2018) 21603–21616.

[76] J.A. Clum, The role of hydrogen in dislocation generation in iron alloys, Scr. Metall. 9 (1975) 51–58.

[77] M. Nagumo, Hydrogen related failure of steels—a new aspect, Mater. Sci. Technol. 20 (2004) 940–950.

[78] M. Nagumo, M. Nakamura, K. Takai, Hydrogen thermal desorption relevant to delay-fracture susceptibility of high-strength steels, Met. Mater Trans A (2001) 339–347.

[79] B. Sun, H. Zhao, X. Dong, C. Teng, A. Zhang, S. Kong, J. Zhou, X. C. Zhang, S. T. Tu, Current challenges in the utilization of hydrogen energy- a focused review on the issue of hydrogen-induced damage and embrittlement, Adv. Appl. Energy 14 (2024) 100168.

[80] G.L. Krasko, G.B. Olson, Effect of hydrogen on the electronic structure of a grain boundary in iron, Solid State Commun. (1991) 113-117.

[81] V.G. Gavriljuk, V.N. Shivanyuk, B.D. Shanina, Change in the electron structure caused by C, N and H atoms in iron and its effect on their interaction with dislocations, Acta Mater. 53 (2005) 5017–5024.

[82] V.G. Gavriljuk, V.N. Shyvaniuk, Teus, Mobility of dislocations in the iron-based C-, N-, H-solid solutions measured using internal friction: effect of electron structure, J. Alloys Compd. 886 (2021) 161260.

[83] P. Bastien, Azou, Influence de l'écrouissage sur le frottement intérieur du fer et de l'acier, chargés ou non en hydrogène, Comptes Rendus Séances Académie Sci. 232 (1951) 1845–1848.

[84] S.M. Teus, V.G. Gavriljuk, On a correlation between the hydrogen effects on atomic interactions and mobility of grain boundaries in the alpha-iron. Stage I. A change in the electron structure of the alpha-iron due to hydrogen, Mater. Lett. 258 (2020) 126801.

[85] V. Shivanyuk, V. Gavriljuk, J. Foct, Effect of hydrogen on interatomic bonds in austenitic steels, Hyperfine Interact. 168 (2006) 1041–1045.

[86] B.D. Shanina, V.G. Gavriljuk, S.P. Kolesnik, V.N. Shivanyuk, Paramagnetic spin resonance in hydrogen-charged stainless austenitic steel, J. Phys. Appl. Phys. 32 (1999) 298-304.

[87] G. Grimvall, The electron-phonon interaction in normal metals, Phys. Scr. 14 (1976) 63-78.

[88] P.L. Rossiter, The electrical resistivity of metals and alloys, Cambridge University Press, Cambridge, 1987.

[89] A.E. Pontini, J.D. Hermida, X-ray diffraction measurement of the stacking fault energy reduction induced by hydrogen in an AISI 304 steel, Scr. Mater. 37 (1997) 1831-1837.

[90] N.I. Noskova, V.A. Pavlov, S.A. Nemnonov, Comparison of stacking-fault energy with metal electron structure, Fiz Met Met. 20 (1965) 920–924.

[91] R.A. Brown, A dislocation model of grain boundary electrical resistivity, J. Phys. F Met. Phys. 7 (1977) 1477-1488.

[92] T. Matsuo, J. Yamabe, H. Furukawa, K. Seki, K. Shimizu, S. Watanabe, S. Matsuoka, Development of new strain gage for high-pressure hydrogen gas use, Exp. Mech. 54 (2014) 431–442.

[93] M. Sajdak, J. Tobola, T. Parashchuk, M. Krzywiecki, P. Powroźnik, K.T. Wojciechowski, Probing hydrogen content in steel using the thermoelectric effect, Chem. Eng. J. 485 (2024) 149735.

[94] W. Raczysnki, D. Elefant, Electrical resistance of hydrogen charged zone-melted and Armco iron in a magnetic field at 20 K, Phys. Status Solidi A 14 (1972) 39–42.

[95] S. Moriya, S. Takaki, H. Kimura, Resistivity recovery at low temperatures in high-purity iron charged with hydrogen, Mater. Sci. Eng. 32 (1974) 71–79.

[96] V.G. Gavriljuk, B.D. Shanina, V.N. Shyvanyuk, S.M. Teus, Hydrogen embrittlement of austenitic steels: electron approach, Corros. Rev. 31 (2013) 33–50.

[97] S. Evers, C. Senöz, M. Rohwerder, Hydrogen detection in metals: a review and introduction of a Kelvin probe approach, Sci. Technol. Adv. Mater. 14 (2013) 014201.

[98] N. Bowler, Four-point potential drop measurements for materials characterization, Meas. Sci. Technol. 22 (2010) 012001.

[99] R.A. Matula, Electrical resistivity of copper, gold, palladium, and silver, J. Phys. Chem. Ref. Data 8 (1979) 1147–1298.

[100] N. Bowler, Y. Huang, Model-based characterization of homogeneous metal plates by four-point alternating current potential drop measurements, IEEE Trans. Magn. 41 (2005) 2102–2110.

[101] K.S. Dieter, Resistivity, in: semiconductor material and device characterization, John Wiley & Sons, Ltd, (2005) 1–59.

[102] H. Bishara, M. Ghidelli, G. Dehm, Approaches to measure the resistivity of grain boundaries in metals with high sensitivity and spatial resolution: a case study employing Cu, ACS Appl. Electron. Mater. 2 (2020) 2049–2056.

[103] ASTM B193-02, Standard test method for resistivity of electrical conductor materials, ASTM International, West Conshohocken, PA, USA, (2016).

[104] A. Giri, J.T. Gaskins, L. Li, Y.S. Wang, O.V. Prezhdo, P.E. Hopkins, First-principles determination of the ultrahigh electrical and thermal conductivity in free-electron metals via pressure tuning the electron-phonon coupling factor, Phys Rev B 99 (2019) 165139.

[105] I. Bakonyi, Accounting for the resistivity contribution of grain boundaries in metals: critical analysis of reported experimental and theoretical data for Ni and Cu, Eur. Phys. J. Plus 136 (2021) 410.

[106] A. Bag, D. Delbergue, P. Bocher, M. Lévesque, M. Brochu, Statistical analysis of high cycle fatigue life and inclusion size distribution in shot peened 300M steel, Int. J. Fatigue 118 (2019) 126–138.

[107] A. Zafra, Z. Harris, C. Sun, E. Martínez-Pañeda, Comparison of hydrogen diffusivities measured by electrochemical permeation and temperature-programmed desorption in cold-rolled pure iron, J. Nat. Gas Sci. Eng. 98 (2022) 104365.

[108] S. Ando, K. Yamakawa, Proceedings of the annual meeting of the japan society of mechanical engineers /MMD, Japan society of mechanical engineers, Tokyo, (1991) 473-478.

[109] H. Fuji, T. Fujishiro, T. Hara, Effect of ammonium thiocyanate on hydrogen entry behavior of low alloy steel under galvanostatic cathode charging, ISIJ Int. 61 (2021) 1151–1158.

[110] K.R. Sriraman, S. Brahimi, J.A. Szpunar, S. Yue, Hydrogen embrittlement of Zn-, Zn–Ni-, and Cd-coated high strength steel, J. Appl. Electrochem. 43 (2013) 441–451.

[111] M. Watanabe, N. Fujimoto, Y. Takeuchi, T. Sawada, Optimization of test conditions for evaluating hydrogen embrittlement susceptibility of high-strength steel for prestressed concrete poles, J. Test. Eval. 50 (2022) 601–612.

[112] S. Frappart, X. Feaugas, J. Creus, F. Thebault, L. Delattre, H. Marchebois, Study of the hydrogen diffusion and segregation into Fe–C–Mo martensitic HSLA steel using electrochemical permeation test, J. Phys. Chem. Solids 71 (2010) 1467–1479.

[113] C.A. Zapffe, C.E. Sims, Hydrogen embrittlement, internal stress and defects in steel, Am. Inst. Min. Metall. Eng. 145 (1941) 225–271.

[114] Mohd.Y. Bin Zakaria, Stack-cracking due to hydrogen embrittlement in a welded pipeline steel, Doctoral thesis, The University of Manchester, United Kingdom, (1989).

[115] C. Hüter, S. Dang, X. Zhang, A. Glensk, R. Spatschek, Effects of aluminum on hydrogen solubility and diffusion in deformed Fe-Mn alloys, Adv. Mater. Sci. Eng. (2016) 4287186.

[116] G. Ming, R.P. Wei, Quasi-cleavage and martensite habit plane, Acta Metall. 32 (1984) 2115–2124.

[117] C.C. Kinney, K.R. Pytlewski, A.G. Khachaturyan, J.W. Morris, The microstructure of lath martensite in quenched 9Ni steel, Acta Mater. 69 (2014) 372–385.

[118] A. Nagao, C.D. Smith, M. Dadfarnia, P. Sofronis, I.M. Robertson, The role of hydrogen in hydrogen embrittlement fracture of lath martensitic steel, Acta Mater. 60 (2012) 5182–5189.

[119] T. Asaoka, Hydrogen trapping behavior in plain carbon and Cr-Mo alloy steel, Met. Hydr. Syst., Pergamon, (1982) 197–204.

[120] H. Peisl, Lattice strains due to hydrogen in metals, in: hydrogen in metals I: basic properties, Springer, Berlin, Heidelberg, (1978) 53–74.

[121] Y. Kagan, A.P. Zhernov, Contribution to the theory of electric conductivity of metals with nonmagnetic impurities, J. Exptl. Theoret. Phys. U.S.S.R 23 (1966) 1107–1123.

[122] H. Asahi, M. Ueno, T. Yonezawa, Prediction of sulfide stress cracking in high-strength tubulars, Corr. 50 (1994) 537–545.